Oncogenic Ras-driven Dorsal/NF-κB signaling contributes to tumorigenesis in a *Drosophila* carcinoma model

Caroline Dillard[1,2], Jose Teles Reis[1,2], Ashish Jain, Roland Le Borgne[3], Heinrich Jasper[4], Tor Erik Rusten [1,2]☑

[1]Center for Cancer Cell Reprogramming, Institute of Clinical Medicine, Faculty of Medicine, University of Oslo, Oslo, Norway

[2]Department of Molecular Cell Biology, Institute for Cancer Research, Oslo University Hospital, Oslo, Norway

[3] Univ Rennes, CNRS-UMR 6290, Institut de Génétique et Développement de Rennes, Rennes, France

[4]Buck Institute for Research on Aging, 8001 Redwood Boulevard, Novato, CA 94945-1400, USA

*Corresponding authors: t.e.rusten@medisin.uio.no, cmdillar@uio.no

Abstract:

Cancer-driving mutations synergize with inflammatory stress signaling pathways during carcinogenesis. *Drosophila melanogaster* tumour models are increasingly recognized as models to inform conserved molecular mechanisms of tumorigenesis with both local and systemic effects of cancer. Although initial discoveries of the Toll-NFκB signaling pathway in development and immunity was pioneered in *Drosophila*, limited information is available for its role in cancer progression. Using a well-studied cooperative Ras^{V12} -driven epithelial-derived tumour model, we here describe functions of Toll- NF-κB signaling in malignant Ras^{V12}, $scrib^{-}$ tumors. The extracellular Toll pathway components ModSP and PGRP-SA and intracellular signaling Kinase, Pelle/IRAK, are rate-limiting for tumor growth. The Toll pathway NFκB protein Dorsal, as well as *cactus/IκB* show elevated expression in tumors with highest expression in invasive cell populations. Oncogenic Ras^{V12}, and not loss of *scribble,* confers increased expression and heterogenous distribution of two Dorsal isoforms, DorsalA and DorsalB in different tumour cell populations. Mechanistic analyses demonstrates that Dorsal drives growth and malignancy by suppressing differentiation, counteracting apoptosis and promoting invasion of Ras^{V12}, $scrib^{-}$ tumors genetically dependent on *twist* and *snail*.

Introduction:

Inflammation, defined as the body's response to harmful external inputs, is a hallmark of cancer [1]. This response is mediated by four major inflammatory pathways: the MAPK, PI3K-AKT, JAK-STAT and NF-κB (canonical and non-canonical) signaling pathways which integrate intra- and extracellular alarms and trigger cellular responses [2]. NF-κB activation has been observed in many cancers [3, 4] and correlates with a poor prognosis in breast and non-small cell lung cancer

44 [5, 6]. NF-κB functions appear cancer-relevant, as a significant body of *in vitro* studies reports its
45 involvement in cellular processes such as invasion [7-9], proliferation [10, 11], stemness [12],
46 survival [10-12] and chemoresistance [12-15]. Similarly, a limited number of human cancer
47 xenograft studies demonstrated a positive effect of NF-κB on cancer proliferation [11], survival
48 [11] and metastatic behavior [8, 9].

49 Despite several attempts, pharmaceutical targeting of NF-κB in cancer has proven
50 ineffective due to toxicity resulting from its essential role in regulating cellular and innate immunity
51 at the organismal level [16, 17]. Therefore, understanding both the upstream and downstream
52 mechanisms governing NF-κB activation and functions in cancer, as well as deciphering whether
53 such mechanisms are specific to cancer cells, is crucial. This understanding may facilitate the
54 design of NF-κB -targeting cancer therapies that spare healthy cells. *In vivo* studies would be
55 informative for achieving this goal.

56 *Drosophila melanogaster* is increasingly being used to study both cancer cell- autonomous
57 mechanisms as well as the biology of complex local and systemic paraneoplastic effects
58 instigated by tumor growth [18]. Among the *Drosophila melanogaster* cancer models, the Ras^{V12},
59 $scrib^{-/-}$ carcinoma model, arising from the concomitant expression of the constitute activated
60 oncogenic form of the KRAS/NRAS orthologue, Ras85D (here referred to as Ras^{V12}), and the loss
61 of cell polarity through *scribble* loss-of-function, has been most extensively studied and displays
62 a remarkable array of hallmarks similar to human cancer [19] [20]. In Ras^{V12}, $scrib^{-/-}$ tumors,
63 generated in the larval eye-antennal disc epithelium (EAD), the evolutionarily conserved Ras-
64 MAPK, PI3K-AKT and JAK-STAT inflammatory pathways all constitute major drivers [19, 20].
65 Surprisingly, at the organismal level, Ras^{V12}, $scrib^{-/-}$ tumour-bearing flies also display both
66 microenvironmental and systemic alterations that mimic human cancer, such as wasting of
67 adipose and muscle tissues, gut atrophy, microenvironmental extracellular matrix remodeling and
68 immune cell infiltration [21-24]. Although the discovery and functions of the Toll-NF-κB and IMD-

69 NF-κB pathways were pioneered in flies and found to control developmental patterning and
70 infection response of the innate immune system [25-27], less information is available for its
71 possible roles in carcinogenesis.

72 Here, we describe the aberrant expression and function of a NF-kB transcription factors in
73 the *Ras*^{V12}*; scrib*$^{-}$ tumour model. We demonstrate that in *Ras*^{V12}*; scrib*^{IR} tumours, the NF-kB
74 transcription factor Dorsal (Dl) plays a pro-tumorigenic role by opposing differentiation and
75 promoting survival and invasion. In this context, Dorsal can amplify JNK signaling activation, a
76 known driver of invasion in this model. We also found that the known Dorsal targets *snail* and
77 *twist* contribute to tumour growth. Interestingly, we report the expression of two different splicing
78 variants of Dl, DorsalA (DlA) and DorsalB (DlB), in non-overlapping tumour cell populations.

79

80 Results

81 **The Toll pathway promotes tumour growth in an autonomous manner**

82 To identify potential tumour-driving mechanisms, we surveyed upregulated genes in
83 *Ras*^{V12}*; scrib*$^{-/-}$ malignant tumours by RNA Sequencing (Fig 1A). We identified 364 genes with
84 elevated expression levels. These include 14 previously identified genes with defined functions in
85 driving *Drosophila* tumor growth or paraneoplastic effects, like organ wasting and diuretic
86 dysfunction (Table 1). Notably, among the upregulated genes - PGRP-SA, GNBP2, Easter, Spz3,
87 and Spz5 - encode extracellular components of the Toll pathway (Fig 1A). The Toll pathway, one
88 of the two established NF-kB signaling pathways in *Drosophila*, is differentially activated during
89 development and in response to fungal or bacterial infection. PGRP-SA (Peptidoglycan
90 Recognition Protein SA) is a secreted protein that binds to bacteria-derived peptidoglycans upon
91 bacterial infection, forming a trimeric complex with a member of the GNBP family (Gram-Negative

92 Binding Protein) and the serine protease ModSP (Modular Serine Protease). This association
93 initiates a multi-step proteolytic cascade, eventually cleaving the ligand Spz (Spaetzle).
94 Subsequently Spz binds to the Toll receptor, activating the Toll pathway intracellularly (Fig 1B).
95 To date, six Spz ligands and nine Toll receptors have been identified and the functions and
96 associations of the different ligands and receptors is not yet fully understood [27]. Intracellularly,
97 Toll receptor activation triggers the activation and formation of a complex composed of the
98 adaptor proteins Myd88 and Tube as well as the serine-threonine protein kinase Pelle. Pelle
99 subsequently phosphorylates the inhibitor Cactus, the homolog of mammalian IkappaB, which is
100 targeted to proteasome degradation. As Cactus sequesters the NF-kB Dorsal or Dif into the
101 cytoplasm, its degradation triggers the translocation of the NF-kBs into the nucleus and the
102 transcription of their target genes (Fig 1B).

103 We decided to first investigate whether PGRP-SA is involved in Ras^{V12}; $scrib^{-/-}$
104 tumorigenesis. To do so, we genetically induced the formation of Ras^{V12}; $scrib^{-/-}$ tumours from
105 randomly induced single cells in the Eye-Antennal Disc (EAD) of the *Drosophila* larva. This way,
106 we can knockdown or overexpress any gene of interest within the tumour specifically without
107 affecting expression in the rest of the body (Fig 1C). To improve RNA interference (IR) expression
108 levels and processing respectively, knockdown experiments were sometimes performed at 29°C
109 with the additional expression of Dicer-2, as indicated in the legends.

110 Knock-down of PGRP-SA ($PGRP\text{-}SA^{IR}$) significantly reduced Ras^{V12}; $scrib^{-/-}$ tumour growth
111 compared to control tumours (Fig 1D). Similarly, knock-down of ModSP ($ModSP^{IR}$) significantly
112 decreased tumour size (Fig 1E), suggesting that the extracellular components of the Toll pathway
113 surprisingly play a pro-tumorigenic role in this context. To address whether Toll signaling is
114 required within tumour cells or in another microenvironmental compartment, we performed knock-
115 down of the intracellular kinase Pelle/IRAK ($pelle^{IR}$), a hub in Toll signal transduction. $pelle^{IR}$
116 Ras^{V12}; $scrib^{-/-}$ tumours exhibited a drastic size reduction compared to control tumours (Fig 1F).

117 These results collectively suggest that *Ras*^{V12}*; scrib*$^{-/-}$ tumours produce extracellular Toll-activating
118 components that contribute to a Toll pathway pro-tumorigenic signal activity in an autonomous
119 manner.

120 **Dorsal is ectopically expressed in oncogenic *Ras*^{V12}-driven tumours**

121 Toll pathway activation leads to the release and nuclear translocation of the NF-κB
122 transcription factors Dl and/or Dif, leading to transcription of target genes. While most studies of
123 Dl and Dif in developmental patterning and infection have focused on their main splicing variants
124 (DlA and DifA), both NF-kB transcription factors have been reported to also have alternatively
125 spliced B isoforms (DlB and DifB) [28, 29]. For instance, both DlA (678 amino acids) and DlB (994
126 amino acids) contain a Relish-homology domain, composed of a DNA binding domain and a
127 dimerization domain (for homo/heterodimerization and Cactus binding), as well as a
128 transactivation domain (for transcription activation) [28]. However, the transactivation domain of
129 DlA is much shorter than Dorsal-B. Noteworthy, only DlA possesses an NLS sequence. Therefore,
130 DlB cannot translocate to the nucleus by itself but is thought to be able to bind to DlA for
131 translocating to the nucleus of fat body cells upon infection [28]. Contrary to DlA, DlB is not
132 expressed and involved in embryonic dorso-ventral patterning. It is rather specifically expressed
133 in the subsynaptic reticulum of neuromuscular junctions, where it stabilizes Cactus. Similarly, Dif-
134 B is found in the mushroom body of the CNS, where it also stabilizes Cactus [29]. Although these
135 observations support the idea that B isoforms play a specific role in nervous system tissues, their
136 precise functions remain to be elucidated [30].

137 We began by assessing the expression of Dl in *Ras*^{V12}*; scrib*^{IR} tumours through
138 immunostainings against DlA and DlB (Fig 2A, 2B, 2C, 2D and S1A, S1B Fig). Both Dorsal
139 isoforms were highly expressed in tumors in the posterior part of the disc that attaches to the brain
140 through the prospective optic stalk (Fig 2A and 2B), while neither DlA or DlB proteins were
141 observed in control clones (Fig 2A). DlA and DlB were almost entirely mutually exclusive, in

142 different cell populations (Fig2A, 2B and S1B Fig). Within *Ras^{V12}; scrib^{IR}* tumours, cells can be
143 easily separated according to their levels of DlA mean intensity (Fig 2C). We identified a DlA^{high}
144 cell population that had four-fold higher DlA protein levels compared to the DlA^{low} remaining cell
145 population. Importantly, the DlA mean intensity in the DlA^{low} cell population was consistently
146 higher than in the surrounding *wt* epithelial cells of the EAD (Fig 2C). These observations suggest
147 that although we observed a peak of DlA expression at the posterior part of the tumour, there is
148 a general elevation of the basal level of DlA throughout the entire tumour. In contrast, we did not
149 observe a general elevation of DlB throughout the tumour when compared to *wt* cells of the TME,
150 but we did observe a local increase in the posterior part of the tumour of a similar magnitude to
151 DlA (Fig 2B and 2D). Tumour cells located in the posterior area of the tumour are closest to the
152 CNS, which is the first organ these tumours invade [31-33]. Intriguingly, tumour cells that have
153 initiated invasion into the optic lobes (OL) of the CNS displayed high levels of DlA or DlB (S1B
154 Fig), suggestive of a potential role of Toll-NFκB signaling in tumor cell migration.

155 Finally, a strong enrichment of the repressor Cactus, the ortholog of mammalian IkappaB
156 (IKKB), was observed in DlA^{high} tumour cells but not in DlB^{high} tumour cells, as assessed with an
157 endogenous GFP fusion protein reporter, *Cactus::GFP* (S1C Fig). This is particularly interesting
158 as *cactus* is a positive transcriptional target of the Toll pathway[34]. Cactus upregulation
159 constitutes a negative feedback loop which could cap Toll pathway activation, a mechanism that
160 has also been described in mammalian NF-kB signalling pathways [35, 36]. In conclusion,
161 simultaneous elevation of DlA, DlB and Cactus expression suggests that in the posterior part of
162 *Ras^{V12}; scrib^{IR}* tumours, Toll pathway activation is significantly higher than in the rest of the tumour.

163 **Dorsal aberrant accumulation is genetically and spatiotemporally-regulated**

164 We investigated what could be the upstream mechanism leading to aberrant Dl
165 accumulation. Initially, we examined Dl isoforms levels in various genetic backgrounds: control

166 *wild type* clones, *scrib*^{IR} tumours, *Ras*^{V12} tumours and *Ras*^{V12}*; scrib*^{IR} tumours. We observed
167 aberrant expression of DlA as well as DlB exclusively in *Ras*^{V12} and *Ras*^{V12}*; scrib*^{IR} tumours (Fig
168 2A), suggesting that *Ras*^{V12} instructs tumour cells competent to produce these isoforms at
169 abnormal levels. Furthermore, we followed DlA levels over time in *Ras*^{V12}*; scrib*^{IR} tumours, using
170 an endogenous Dorsal genetic reporter, that acts as a Dorsal-A specific reporter in this context
171 (Fig 3A and S2A and S2B Fig). The onset of DlA expression correlated with the appearance of
172 Elav-positive neurons in the prospective eye region of the tumours around Day5 (Fig 3A).
173 Interestingly, DlA accumulate in cells surrounding the neurons but was rarely detected in the
174 neurons themselves (Fig 3A yellow arrows and Fig 3B). Concurrently, DlB expression was
175 exclusive to the tumour neurons (Fig 3C). Within the tumours, apoptosis was predominantly
176 observed in the differentiating areas where we observed dying neurons (Fig 3D, yellow arrows).
177 Therefore, we hypothesized that the local aberrant Dl expression might be triggered by cell death-
178 derived signals. However, efficient blocking of apoptosis in *Ras*^{V12}*; scrib*^{IR} tumours through Diap1
179 overexpression (*Diap1*^{OE}) did not affect increased DlA and DlB levels (Fig 3E and 3F).

180 Together, these observations demonstrate that the aberrant expression NF-kB/Dl in
181 *Ras*^{V12}*; scrib*^{IR} tumours is both genetically and locally controlled. General elevated levels of DlA in
182 the whole tumor population suggests a transcriptional response downstream of oncogenic Ras^{V12}
183 signaling. On top of this Ras^{V12}-dependent genetic control, a temporal and or local control triggers
184 elevated levels of DlA, DlB and Cactus specifically in the posterior part of the tumour in the
185 prospective eye region, as well as in invading tumour cells to the brain.

186 **Dorsal represses Ras^{V12} scrib^{IR} tumour differentiation and death**

187 To investigate the primary functions of Dl in *Ras*^{V12}*; scrib*^{IR} tumours, we conducted
188 knockdown experiments using two independent RNAis that efficiently target both Dorsal isoforms
189 (S3A and S3B Fig). *Dorsal*^{IR}*, Ras*^{V12}*; scrib*^{IR} tumours exhibited a significant reduction in size
190 compared to *Cherry*^{IR} *Ras*^{V12}*; scrib*^{IR} control tumours (Fig 4A), mimicking the phenotypes

191 observed upon *PGRP-SA*, *ModSP* and *pelle* knockdowns (Fig1C, 1D and 1E). *Ras*^{V12}*; scrib*^{IR}
192 tumour growth results from a combination of cell growth, cell proliferation, inhibition of the
193 differentiation of epithelial tumour cells into Elav-positive photoneurons and survival [31, 37]. To
194 delineate the potential functions of Dl in *Ras*^{V12}*; scrib*^{IR} tumours, we assessed alterations in
195 proliferation, differentiation and apoptosis. Quantification of mitotic cells suggests that *Dorsal*^{IR}
196 *Ras*^{V12}*; scrib*^{IR} tumours display similar proliferation rates to control tumours, but both their
197 differentiation and apoptosis rates were significantly higher than in control tumours (Fig4B, 4C
198 and 4D). Although, a few neurons form in *Ras*^{V12}*; scrib*^{IR} tumours, they appeared spaced apart
199 and did not form the full complement of eight neurons per ommatidia. However, upon Dorsal
200 knockdown, Elav-positive cells increased in number and density, suggesting a partial rescue of
201 differentiation (Fig4C). The fact that we frequently observed cell death coinciding with areas
202 where Elav-positive neurons were present (Fig 3D) suggests that cell death might be a
203 consequence of aberrant tumour cell differentiation. Importantly, *Pelle*^{IR} *Ras*^{V12}*; scrib*$^{-/-}$ tumours
204 also exhibited increased apoptosis and differentiation rates (S3C Fig). This emphasizes the need
205 for the Toll signalling pathway, and not an alternative way to activate Dorsal/NFkB activity, to
206 promote tumour growth. Thus, the Toll-Dl signaling pathway promotes tumour growth primarily by
207 preventing differentiation and promoting survival.

208 **Dorsal is required for invasion and accentuates JNK signaling**

209 We next addressed whether Dl is involved in tumor invasion. In the *Ras*^{V12}*; scrib*^{IR} tumour
210 model, cells adopt a migratory behavior by JNK signaling. Specifically, JNK mediates expression
211 of Matrix MetalloProteinase 1 (MMP1) and Cheerio (Cher-mammalian Filamin), resulting in
212 basement membrane degradation and cytoskeleton remodeling respectively [22, 32, 37-41]. We
213 conducted colocalization analyses, assessed by the Pearson's Correlation Coefficient (PCC),
214 between the Dorsal isoforms and JNK activity in the tumours, assessed either through activated
215 JNK (phosphor-JNK, pJNK) or a JNK activity reporter, TRE-eGFP. Overall, we found a low

216 colocalization between DlA and TRE-eGFP (Fig 5A) while we observed a good PCC between DlB
217 and pJNK within the tumours (Fig 5B). These observations align with the finding that tumor cells
218 invading the CNS often have high levels of either DlA or DlB.

219 To test whether Dorsal may function upstream of JNK signaling in *Ras*^{V12}*; scrib*^{IR} tumours, we
220 assessed the levels of the JNK target MMP1 following *Dorsal*^{OE} and *ModSP*^{OE} overexpression
221 which enhances Toll signaling and subsequently Dorsal activity. MMP1 mean intensity was
222 significantly higher in tumors with elevated *Dorsal* or *ModSP* expression. compared to control
223 tumours. Therefore, Toll-Dl signaling can augment expression of the JNK transcriptional target,
224 *mmp1* in *Ras*^{V12}*; scrib*^{IR} tumours (Fig 5C).

225 As both DlA, DlB and Cactus are highly expressed in brain lobe proximal and invading cells and
226 Dl amplifies JNK signalling in the tumours, we investigated the effect of Dorsal knock-down on
227 tumour cell migration. We scored for three parameters reflecting the mobility of tumour cells at
228 late stages of tumour development (Day 12): 1/ the VNC invasion score, which assigns a higher
229 score to tumors with greater migration toward the tip of the ventral nerve cord (VNC) of the CNS,
230 2/the frequency at which we observe tumour cells within the organs adjacent to the VNC called
231 leg discs and 3/ the fusion of tumours generated in the two distinct EAD, indicating the ease with
232 which cells move from one EAD to the other and EADs and come into contact with each other
233 (Fig 6A). To mitigate the influence of tumour cell number on migration assessment, we compared
234 control and *Dorsal*^{IR} tumours of similar size. Upon Dorsal knock-down, at late stages, the three
235 parameters showed a drastic decrease: the VNC score decreased threefold compared to control,
236 reaching a low value similar to early-stage control tumours (Fig6B). The frequency of invasion
237 into leg discs decreased sevenfold and tumors from neighboring EADs often failed to merge (Fig
238 6A). Similarly, Dorsal overexpression (*Dorsal*^{OE}) increased tumour cell mobility even at early
239 stages (Day 6), while tumour size is signicantly smaller (Fig 6B), suggesting that 1/ the increase
240 in invasion is not simply a secondary consequence of higher cell number and 2/ that the balance

241 between invasion and tumour growth tilted toward invasion when tumour cells have high levels of
242 Dorsal.

243 Given the functions of Dorsal in the tumour context, we wondered whether *Dorsal*^{OE} is sufficient
244 to induce tumorigenesis. Although, *Dorsal*^{OE} control clones were not bigger than *wt* clones, we
245 systematically observed the formation of dysplasic GFP-labeled *Dorsal*^{OE} clones within the EADs
246 that appeared as large-rounded cell masses often located basally (S4A and S4B Fig, yellow
247 arrow). We hypothetize that they arise from the inhibition of differentiation. Moreover, in this
248 context, we never observed *Dorsal*^{OE} cells in the VNC (VNC score in S4A Fig). Thus, Dorsal at
249 high levels is sufficient to trigger dysplasia but not invasive hyperplastic tumours.

250 The Epithelial-to-Mesenchymal (EMT) transcription factor Snail has been implicated in
251 promoting invasion of *Ras*^{V12}*; lgl*$^{-/-}$ tumours (a similar tumour model to *Ras*^{V12}*; scrib*$^{-/-}$ tumours)
252 through stimulation of JNK signaling and EMT-like cytoskeleton remodeling [42]. Snail, along
253 with Twist, another EMT transcription factor, are well-known targets of Dorsal that govern
254 mesoderm invagination during developmental patterning in cells with the highest Dorsal activity
255 [43-46]. Interestingly, knockdowns of both Snail and Twist significantly decreased *Ras*^{V12}*; scrib*^{IR}
256 tumour size (S4A and S4B Fig), mimicking Dorsal knockdown. At late stages, twistIR *Ras*^{V12}*;*
257 *scrib*^{IR} tumour also displayed a lower VNC score compared to control tumours, suggesting
258 impaired tumour cell migration (S4B Fig). We propose a model where the Dl^{high} tumour cells
259 activate Twist and Snail expression, provoking migration, in part through JNK signalling
260 enhancement (Fig 7A).

261 Taken together, these experiments suggest that Dl promotes tumor growth through
262 repressing cell death and differentiation as well as promoting EMT like delamination and invasion
263 dependent on Twist and Snail activity.

264 Conclusion/Discussion

265 Here, we establish that autonomous activation of the inflammatory Toll pathway plays a pivotal
266 role in supporting the growth of *Ras^{V12}; scrib^{IR}* tumours. The NF-kB transcription factors Dorsal,
267 and key effectors of the Toll pathway, exhibit aberrant expression in this model. In this context,
268 Dorsal activity facilitates tumour growth by preventing differentiation and promoting survival
269 without measurable impact on proliferation. Additionally, Dorsal promotes invasion genetically
270 dependent on the EMT factors Snail and Twist.

271 An exciting feature in this tumor model is tumor heterogeneity in both NF-kB protein composition
272 (DlA and DlB) and Toll pathway activity (Dl^{high} cactus^{high} vs Dl^{low}, Cactus^{low}), as judged by classical
273 target gene expression (*cactus* and *dorsal*) and stimulation of invasion. Dl is unevenly
274 accumulated within the population of transformed cells in a spatial and regional manner and on
275 at least two levels: there is a low-level DlA accumulation within the entire region of Ras^{V12}
276 expression and a heightened level in the posterior region situated in the differentiating prospective
277 eye region that is physically attached to the brain through the stalk. In this region a notable
278 accumulation of both splicing variants of Dl, DlA and DlB, is seen within distinct tumour cell
279 populations.

280 While NF-kB protein heterogeneity within the same tumour has not been studied yet in
281 solid mammal tumours, the NF-kB fingerprinting and their subsequent homo-/heterodimerization
282 within diffuse large B-cell lymphoma hold predictive values for the tumour cell response to
283 microenvironmental activating cues [47]. With our study, this finding, suggest that NF-kB
284 composition heterogeneity might also occur in solid mammal cancers and modulate their
285 response to microenvironmental inflammation.

286 Moreover, heterogeneity in the level/activity of a single NF-kB mirrors observations in mammalian
287 cancers. In pancreatic cancer, where oncogenic KRAS is the main driver, tumor heterogeneity is
288 a central hallmark and frequently associated with variable NF-kB signaling. A central question is
289 thus, what causes some cells to respond with inflammation whereas others do not? Possibilities

290 include non-autonomous external input from nearby cells of the microenvironment or circulation
291 versus intrinsic mechanisms. *In vitro* studies of $KRAS^{G12V}$-transfected immortalized human
292 pancreatic epithelial derived cells (HPDE) have demonstrated that variable levels of oncogenic
293 KRAS can produce different outcomes. High $KRAS^{G12V}$ expression can direct NF-kB signaling
294 and EMT phenotypes driven in part by feed forward loop through IL6 signaling, whereas lower
295 level of KRAS activity retains epithelial character with lower level of NF-kB signaling dependent
296 on IL1 [48].

297 In the Ras^{V12}, $scrib^{-/-}$ model, a "flip out" cassette turns on Ras^{V12} expression under control
298 of the actin promoter in all cells with the same genetic dose, and by first principle should signal
299 evenly. Yet, Ras^{V12} - driven NF-kB expression is temporally and spatially controlled in a
300 stereotypic pattern. One possibiity is that this region is prepatterned to respond to increased levels
301 of Ras^{V12} with a higher response. Indeed, in this region, we observe a higher level of pMAPK and
302 where tumour region neurogenesis is incomplete as we do not observe fully formed ommatidia
303 emphasizing the inhibitory effect of Dorsal on differentiation. In the prospective eye region, behind
304 the morphogenetic frurrow, founder R8 neurons recruit further neurons through Receptor Tyrosine
305 Kinase-MAPK signaling that potentially could add up with Ras^{V12}-MAPK signaling to reach a
306 higher signaling levels [49].

307 Extrinsic regulation of Toll signaling does have a role in the Ras^{V12}, $scrib^{-/-}$ tumor model for growth.
308 The Toll-activating components implicated in tumour growth, PGRP-SA and ModSP, are part of
309 a bacterial recognition alert system. The observed overexpression of PGRP-SA in Ras^{V12}; $scrib^{IR}$
310 tumours may serve to locally increase the concentration of active cleaved Spz ligands, thereby
311 stimulating Toll activation and promoting tumor growth. The source of activation governed by
312 PGRP-Sa and ModSP remains unknown. As the posterior part of the disc experience higher levels
313 of apoptosis, we considered whether apoptotic cell death and debris could active PGRP-
314 SA/ModSP - driven Toll sigaling in this context through death- induced danger signals and

315 bacterial component mimicry, but inhibition of death through DIAP1 expression did not alter NFkB
316 levels.

317 Notably, previous studies have identified PGRP-SA, Cactus, and Dorsal as positive targets of the
318 Toll pathway [34]. Furthermore, it has been shown that the CNS serves as a significant source of
319 Spz ligands that regulates *Ras*^{V12}*; lgl*$^{-/-}$ tumour migration tropism through Toll6 [33]. Hence, it is
320 tempting to think that upon the onset of neurogenesis, tumour cells suddenly gain access to
321 elevated levels of Spz concentration from the brain, significantly enhancing local Toll activation
322 and subsequent PGRP-SA and Dorsal expression. This hypothesis may explain the spatial
323 restriction of aberrant Dorsal expression to the posterior part of the tumor.

324 We have yet to assess whether DIA and DIB exert different functions within *Ras*^{V12}; *scrib*^{IR}
325 tumours, as our knockdowns and overexpression transgenes targeted both isoforms
326 simultaneously. Consistent with previous reports, DIB expression in the tumor context is restricted
327 to cell types from the nervous system. Colocalization of DIB with pJNK in neurons that seem prone
328 to die, allows us to speculate if both isoforms have distinct functions, that DIB may promote
329 migration through JNK, while DIA may favor stemness and survival. Additionally, we cannot yet
330 rule out the involvement of other NF-kBs, such as Dif and Relish in *Ras*^{V12}*; scrib*^{IR} tumours.

331 Using splicing variants may be a mechanism to diversify the range of NF-kB actions in
332 various contexts in Drosophila, as it possesses only three NF-kBs (Dorsal, Dif, and Relish). In
333 contrast, mammalian NF-kBs are not reported to have splicing variants, although they possess
334 five different NF-kBs. To our knowledge, the concept of intratumoral NF-kB heterogeneity remains
335 relatively unexplored in mammalian cancer biology and the fly model offer an experimentally
336 accessible model to investigate this question *in vivo*. Future research efforts will be crucial in
337 elucidating the importance and mechanisms underlying intratumoral NF-kB heterogeneity during
338 malignant transformation.

339 The Ras^{V12}, scrib tumor model engages five known inflammatory pathways during
340 transformation. Ras^{V12} directly drives MEK-ERK and PI3K-AKT signaling while engaging Toll-
341 NFkB, whereas loss of cell polarity through scribbled, initiates TNFR-JNK MAPK stress signaling
342 and as a result, an Upd/IL6-JAK-STAT autocrine signaling loop altogether favoring malignant
343 transformation.

344 In conclusion, the findings herein extends the understanding of how innate immune signaling is
345 engaged by and cooperates with oncogenic Ras, and opens up for more detailed mechanistic
346 studies in a genetically tractable preclincial tumor model with clear paralells to human cancer

347

348 **Material and Methods**

349 ***Drosophila* lines**

350 The EyMARCM system is known to generate flip-out clones in the adjacent optic lobes of the
351 CNS in addition to the eye discs [50]. For assessing tumour cell migration from true carcinoma
352 cells arising from the eye disc epithelium, we therefore used another genetic system designed in
353 our lab, called EyaHost, that generates flip-out tumours exclusively in the EAD but not in the
354 CNS (to be described in detail elsewhere).

355 Unless otherwise specified, crosses were conducted at 25°C by default; however, for enhanced
356 knockdown efficiency, most knockdown experiments were carried out at 29°C, as detailed in the
357 figures and legends.

358 - EyMARCM Drosophila lines:

359 Ey,flp; act>STOP>Gal4, UAS-GFP; FRT82B Tub-Gal80ts [32]

360 Ey,flp, UAS-Dcr2; act>STOP>Gal4, UAS-GFP; FRT82B Tub-Gal80ts

361 ;Sp/CyO, Dfd-YFP; UAS-Ras^{V12} FRT82B scrib$^{[2]}$/TM6C {Bilder, 2000 #23;Chen, 2012 #24;Perez,
362 2017 #22;Perez-Garijo, 2009 #25}

363 ; UAS-PGRP-SA^{IR}; UAS-Ras^{V12} FRT82B scrib$^{[2]}$/TM6C (BDSC#60037)

364 ; UAS-modSP^{IR}; UAS-Ras^{V12} FRT82B scrib$^{[2]}$/TM6C (VDRC GD#43972)

365 ; UAS-pelle^{IR}; UAS-Ras^{V12} FRT82B scrib$^{[2]}$/TM6C (BDSC#50715)

366 ; UAS-RFP^{IR}; UAS-Ras^{V12} FRT82B scrib$^{[2]}$/TM6C (BDSC#67852)

367 ;UAS-Ras^{V12} ; FRT82B scrib$^{[1]}$/TM6C [51]

368 ;UAS-Ras^{V12} ; FRT82B

369 FRT82B scrib$^{[1]}$/TM6C

370 FRT82B

371 - EyaHost Drosophila lines

372 ; Eya-KD; QUAS-Gal4 (Eya-KD our own lab, QUAS-Gal4 BDSC#83132 {Baena-Lopez, 2018
373 #32})

374 QUAS-Ras^{V12} ; Eya-KD; QUAS-Gal4 (QUAS-Ras^{V12} from Peter Galant)

375 QUAS-Ras^{V12} ; Eya-KD, QUAS-scrib^{IR}; QUAS-Gal4 (QUAS-scrib^{IR} from our own lab)

376 QUAS-Ras^{V12} ; Eya-KD, QUAS-scrib^{IR};

377 QUAS-Ras^{V12} ; Eya-KD, QUAS-scrib^{IR}; QUAS-Gal4, UAS-Dcr2 (UAS-Dcr2 BDSC#24651)

Act>|STOP>|QF, QUAS-mCD8::GFP;; (Act>|STOP>|QF from our own lab, QUAS-mCD8::GFP BDSC#30001)

Act>|STOP>|QF, QUAS-mCD8::GFP; UAS-dorsal; (BDSC#9319)

Act>|STOP>|QF, QUAS-mCD8::GFP; UAS-modSP; (B.Lemaître {Dostalova, 2017 #33})

Act>|STOP>|QF, QUAS-mCD8::GFP; UAS-diap1^{OE}; (BDSC#6657)

Act>|STOP>|QF, QUAS-mCD8::GFP;; UAS-cherry^{IR} (BDSC#35785)

Act>|STOP>|QF, QUAS-mCD8::GFP;; UAS-dorsal^{IR-1} (BDSC#32934)

Act>|STOP>|QF, QUAS-mCD8::GFP;; UAS-dorsal^{IR-2} (BDSC#27650)

Act>|STOP>|QF, QUAS-mCD8::GFP;; UAS-snail^{IR} (VDRC GD#6232)

Act>|STOP>|QF, QUAS-mCD8::GFP;; UAS-twist^{IR-1} (BDSC#51164)

Act>|STOP>|QF, QUAS-mCD8::GFP;; UAS-twist^{IR-2} (BDSC#25981)

Act>|STOP>|QF, QUAS-Tag2BFP;; genomic-dorsal::GFP (BDSC#42677)

Act>|STOP>|QF, QUAS-Tag2BFP;; genomic-cactus::GFP (VDRC fTRG 318145)

Act>|STOP>|QF, Ey-flp, QUAS- Tag2BFP; TRE-eGFP; (QUAS-Tag2BFP our own lab, TRE-eGFP BDSC#59010)

Immunohistochemistry

Inverted larvae heads were fixed 30 min in 4% paraformaldehyde/PBS at room temperature on a shaker. After washes, fine dissection of single EADs (for early-stage tumours at Day 6) or whole

396 cephalic complexes (at later stages) was conducted in PBS. The tissues were then incubated with
397 a solution of primary antibody in 0,5% Triton X-100/PBS overnight at 4°C. Noteworthy, for primary
398 antibodies that presented penetration defects (marked with * below), we incubated the tissues in
399 0,5% Triton X-100/PBS overnight at 4°C prior to primary antibody stainings. Similarly, secondary
400 antibody stainings was done in 0,5% Triton X-100/PBS overnight at 4°C. Samples were then
401 mounted in Vectashield or equivalent mounting media for imaging.

402 Primary antibodies were used at the following dilutions: anti-DIA mouse antibody (1:50, DSHB
403 7A4), anti-DlB rabbit antibody (* 1:1000, S.Wasserman [29]), anti-pH3 rat (1:200 abcam 10543),
404 anti-Elav rat (1:50, DSHB 7E8A10), anti-cleaved Dcp1 rabbit (1:100, Cell Signaling 9578), anti-
405 phosphoJNK mouse (* 1:100, Cell Signaling 9255) and anti-MMP1 mouse (* used in a mix 1:1:1,
406 DSHB 3B8D12, DSHB 3A6B4 and DHSB 5H7B11). Secondary antibodies were all from Jackson
407 ImmunoResearch.

408 **RNA sequencing and data analysis**

409 Third instar larval eye discs of the indicated genotypes were manually isolated and RNA was
410 extracted using Qiagen RNAmini kits. TruSeq RNA Library Prep Kit (Illumina) was used to prepare
411 libraries, and sequencing was performed on an Illumina MiSeq system. Raw data were analyzed
412 with the Tuxedo suite (RRID:SCR_013194) and reads were mapped to Drosophila genome
413 release 5.2. Expression was recorded as FPKM: fragments per kilo-base per million reads.

414

415

416

417 ## Imaging

418 Samples were imaged on Zeiss LSM880 and Zeiss LSM980 confocal microscopes as well as on
419 Nikon HCI SoRa spinning disc microscope. They were further processed on FIJI.

420 ## Tumour Volume Analysis

421 Z-stacks were acquired with a 3µm step for early-stage tumors (Day 6) and a 4µm step for late-
422 stage tumors (after Day 6). Tumor volume was estimated using a FIJI Macro [52], which
423 automatically performs threshold-based 3D reconstruction of the GFP+ signal, followed by
424 volume measurements (3D Object counter plugin). Before 3D reconstruction, the FIJI Macro
425 applies two consecutive Gaussian blur steps (sigma=2) to reduce noise.

426 ## Image processing

427 - Fluorescence intensity measurements and heatmaps

428 Fluorescence intensity measurements were performed using a FIJI Macro, which subtracts
429 background intensity to the signal of interest inside or outside the tumour, using a tumour mask
430 generated from intensity thresholding. When comparing values across different conditions, they
431 were normalized to the mean value of the control condition, ensuring the control mean is set at
432 1. In Fig 2B and Fig 2C, the tumours were split in two compartments “high” and “low”, according
433 to arbitrarily set intensity thresholds (250 for DIA, 10000 for DIB). Normalized mean intensities
434 were then automatically quantified within the different compartments: tumourHigh, tumourLow
435 and TME. DIA and DIB intensity heatmaps were generated after background subtraction, using
436 the Fire LUT in FIJI.

437 - Colocalization analysis

438 Colocalization analyses were performed using a FIJI Macro, which automatically computed the
439 Pearson's Correlation Coefficient (PCC) between two channels of a confocal image using the
440 "coloc2" plugin. The PCC, ranging from -1 to 1, denotes the degree of colocalization between
441 signals. A higher absolute value indicates stronger colocalization, with the sign indicating
442 correlation direction ("-" for anti-correlation, "+" for correlation).

443 - Proliferation, differentiation and apoptosis ratio

444 The proliferation, differentiation and apoptosis ratio are defined as the area of the meaningful
445 marker within the tumour (pH3, Elav and cDcp respectively) divided by the area of the tumour.
446 These ratios were measured with a FIJI Macro which measures both the tumour area and the
447 tumour marker area using an automatic-thresholding. For Fig 3A, 3B and 3C, measurements
448 were conducted on single confocal pictures whereas, for S1 Fig, the apoptosis ratio was
449 measured on the Z-projection of confocal Z-stacks.

450 - Migration score

451 Migration of the VNC and leg discs was manually scored on Z-projection (Max Intensity mode)
452 of confocal Z-stacks.

453 Statistical analyses

454 At least, two biological replicates were performed for each experiment. According to the
455 normality and size of the datasets, appropriate statistical tests were applied using GraphPad
456 Prism9 and are indicated in the figure legends. Graphs were also generated on GraphPad
457 Prism9 and are presented as boxplots (10-90 percentile) or dot plots indicating the mean of the
458 datasets. Statistical significance was categorized as follows: *$p < 0.05$, **$p < 0.01$, ***$p < 0.001$,
459 ****$p < 0.0001$, and n.s when not significant.

Acknowledgement

We thank Drs. Steven A. Wasserman and Amy Kieger, Bruno Lemaitre, the Bloomington Drosophila Stock Center; the Vienna Drosophila Resource Center and the Developmental Studies Hybridoma Bank for providing fly

466 stocks and antibodies. We thank Alicia Alfonso Gomez for help with fly handling, experimental
467 support and image acquisition. We also thank the Core Facilities for Advanced Light Microscopy
468 and Advanced Electron Microscopy at Oslo University Hospital and the Microscopy Rennes
469 Imaging facility of the UMS Biosit, a member of the national infrastructure France-BioImaging,
470 supported by the French National Research Agency (ANR-10-INBS-04).
471 C.D, J.T.R., A.J., T.E.R and were financed by The Norwegian Research Council Toppforsk and
472 Center of Excellence, CanCell grants #262652 and #276070

473

474 Author contributions

475 CD and TER conceived the project and planned experiments. CD, AJ, JTR and H.J. performed
476 experiments and analysis. H.J., and R.L. B. provided feedback to experimental approaches. T.E.R
477 Is the leading principal investigator who together with C.D supervised research and edited the
478 manuscript with input from all coauthors.

479

480

481

482

483

484

485

486

487

488 1. Hanahan D. Hallmarks of Cancer: New Dimensions. Cancer Discov. 2022;12(1):31-46.
489 2. Zhao H, Wu L, Yan G, Chen Y, Zhou M, Wu Y, et al. Inflammation and tumor progression:
490 signaling pathways and targeted intervention. Signal Transduct Target Ther. 2021;6(1):263.
491 3. Aggarwal BB, Sung B. NF-kappaB in cancer: a matter of life and death. Cancer Discov.
492 2011;1(6):469-71.
493 4. Xia L, Tan S, Zhou Y, Lin J, Wang H, Oyang L, et al. Role of the NFkappaB-signaling pathway in
494 cancer. Onco Targets Ther. 2018;11:2063-73.
495 5. Gu L, Wang Z, Zuo J, Li H, Zha L. Prognostic significance of NF-kappaB expression in non-small
496 cell lung cancer: A meta-analysis. PLoS One. 2018;13(5):e0198223.
497 6. Sarkar DK, Jana D, Patil PS, Chaudhari KS, Chattopadhyay BK, Chikkala BR, et al. Role of NF-
498 kappaB as a Prognostic Marker in Breast Cancer : A Pilot Study in Indian Patients. Indian J Surg Oncol.
499 2013;4(3):242-7.
500 7. Boukerche H, Su ZZ, Emdad L, Sarkar D, Fisher PB. mda-9/Syntenin regulates the metastatic
501 phenotype in human melanoma cells by activating nuclear factor-kappaB. Cancer Res. 2007;67(4):1812-
502 22.
503 8. Huang S, Pettaway CA, Uehara H, Bucana CD, Fidler IJ. Blockade of NF-kappaB activity in human
504 prostate cancer cells is associated with suppression of angiogenesis, invasion, and metastasis.
505 Oncogene. 2001;20(31):4188-97.
506 9. Huber MA, Azoitei N, Baumann B, Grunert S, Sommer A, Pehamberger H, et al. NF-kappaB is
507 essential for epithelial-mesenchymal transition and metastasis in a model of breast cancer progression. J
508 Clin Invest. 2004;114(4):569-81.
509 10. Biswas DK, Shi Q, Baily S, Strickland I, Ghosh S, Pardee AB, et al. NF-kappa B activation in human
510 breast cancer specimens and its role in cell proliferation and apoptosis. Proc Natl Acad Sci U S A.
511 2004;101(27):10137-42.
512 11. Cui X, Shen D, Kong C, Zhang Z, Zeng Y, Lin X, et al. NF-kappaB suppresses apoptosis and
513 promotes bladder cancer cell proliferation by upregulating survivin expression in vitro and in vivo. Sci
514 Rep. 2017;7:40723.
515 12. Talukdar S, Das SK, Pradhan AK, Emdad L, Windle JJ, Sarkar D, et al. MDA-9/Syntenin (SDCBP) Is a
516 Critical Regulator of Chemoresistance, Survival and Stemness in Prostate Cancer Stem Cells. Cancers
517 (Basel). 2019;12(1).
518 13. Bentires-Alj M, Barbu V, Fillet M, Chariot A, Relic B, Jacobs N, et al. NF-kappaB transcription
519 factor induces drug resistance through MDR1 expression in cancer cells. Oncogene. 2003;22(1):90-7.
520 14. Bednarski BK, Ding X, Coombe K, Baldwin AS, Kim HJ. Active roles for inhibitory kappaB kinases
521 alpha and beta in nuclear factor-kappaB-mediated chemoresistance to doxorubicin. Mol Cancer Ther.
522 2008;7(7):1827-35.
523 15. Xia YZ, Ni K, Guo C, Zhang C, Geng YD, Wang ZD, et al. Alopecurone B reverses doxorubicin-
524 resistant human osteosarcoma cell line by inhibiting P-glycoprotein and NF-kappa B signaling.
525 Phytomedicine. 2015;22(3):344-51.
526 16. Baud V, Karin M. Is NF-kappaB a good target for cancer therapy? Hopes and pitfalls. Nat Rev
527 Drug Discov. 2009;8(1):33-40.
528 17. Rasmi RR, Sakthivel KM, Guruvayoorappan C. NF-kappaB inhibitors in treatment and prevention
529 of lung cancer. Biomed Pharmacother. 2020;130:110569.
530 18. Bilder D, Ong K, Hsi TC, Adiga K, Kim J. Tumour-host interactions through the lens of Drosophila.
531 Nat Rev Cancer. 2021;21(11):687-700.
532 19. Dillard C, Reis JGT, Rusten TE. Ras(V12); scrib(-/-) Tumors: A Cooperative Oncogenesis Model
533 Fueled by Tumor/Host Interactions. Int J Mol Sci. 2021;22(16).
534 20. La Marca JE, Richardson HE. Two-Faced: Roles of JNK Signalling During Tumourigenesis in the
535 Drosophila Model. Front Cell Dev Biol. 2020;8:42.

536 21. Pastor-Pareja JC, Wu M, Xu T. An innate immune response of blood cells to tumors and tissue
537 damage in Drosophila. Dis Model Mech. 2008;1(2-3):144-54; discussion 53.
538 22. Cordero JB, Macagno JP, Stefanatos RK, Strathdee KE, Cagan RL, Vidal M. Oncogenic Ras diverts
539 a host TNF tumor suppressor activity into tumor promoter. Dev Cell. 2010;18(6):999-1011.
540 23. Khezri R, Holland P, Schoborg TA, Abramovich I, Takats S, Dillard C, et al. Host autophagy
541 mediates organ wasting and nutrient mobilization for tumor growth. EMBO J. 2021;40(18):e107336.
542 24. Holland P, Quintana EM, Khezri R, Schoborg TA, Rusten TE. Computed tomography with
543 segmentation and quantification of individual organs in a D. melanogaster tumor model. Sci Rep.
544 2022;12(1):2056.
545 25. Minakhina S, Steward R. Nuclear factor-kappa B pathways in Drosophila. Oncogene.
546 2006;25(51):6749-57.
547 26. Hetru C, Hoffmann JA. NF-kappaB in the immune response of Drosophila. Cold Spring Harb
548 Perspect Biol. 2009;1(6):a000232.
549 27. Valanne S, Wang JH, Ramet M. The Drosophila Toll signaling pathway. J Immunol.
550 2011;186(2):649-56.
551 28. Gross I, Georgel P, Oertel-Buchheit P, Schnarr M, Reichhart JM. Dorsal-B, a splice variant of the
552 Drosophila factor Dorsal, is a novel Rel/NF-kappaB transcriptional activator. Gene. 1999;228(1-2):233-
553 42.
554 29. Zhou B, Lindsay SA, Wasserman SA. Alternative NF-kappaB Isoforms in the Drosophila
555 Neuromuscular Junction and Brain. PLoS One. 2015;10(7):e0132793.
556 30. Gramates LS, Agapite J, Attrill H, Calvi BR, Crosby MA, Dos Santos G, et al. FlyBase: a guided tour
557 of highlighted features. Genetics. 2022;220(4).
558 31. Brumby AM, Richardson HE. scribble mutants cooperate with oncogenic Ras or Notch to cause
559 neoplastic overgrowth in Drosophila. EMBO J. 2003;22(21):5769-79.
560 32. Pagliarini RA, Xu T. A genetic screen in Drosophila for metastatic behavior. Science.
561 2003;302(5648):1227-31.
562 33. Mishra-Gorur K, Li D, Ma X, Yarman Y, Xue L, Xu T. Spz/Toll-6 signal guides organotropic
563 metastasis in Drosophila. Dis Model Mech. 2019;12(10).
564 34. De Gregorio E, Spellman PT, Tzou P, Rubin GM, Lemaitre B. The Toll and Imd pathways are the
565 major regulators of the immune response in Drosophila. EMBO J. 2002;21(11):2568-79.
566 35. Scott ML, Fujita T, Liou HC, Nolan GP, Baltimore D. The p65 subunit of NF-kappa B regulates I
567 kappa B by two distinct mechanisms. Genes Dev. 1993;7(7A):1266-76.
568 36. Ghosh S, May MJ, Kopp EB. NF-kappa B and Rel proteins: evolutionarily conserved mediators of
569 immune responses. Annu Rev Immunol. 1998;16:225-60.
570 37. Kulshammer E, Mundorf J, Kilinc M, Frommolt P, Wagle P, Uhlirova M. Interplay among
571 Drosophila transcription factors Ets21c, Fos and Ftz-F1 drives JNK-mediated tumor malignancy. Dis
572 Model Mech. 2015;8(10):1279-93.
573 38. Uhlirova M, Bohmann D. JNK- and Fos-regulated Mmp1 expression cooperates with Ras to
574 induce invasive tumors in Drosophila. EMBO J. 2006;25(22):5294-304.
575 39. Srivastava A, Pastor-Pareja JC, Igaki T, Pagliarini R, Xu T. Basement membrane remodeling is
576 essential for Drosophila disc eversion and tumor invasion. Proc Natl Acad Sci U S A. 2007;104(8):2721-6.
577 40. Kulshammer E, Uhlirova M. The actin cross-linker Filamin/Cheerio mediates tumor malignancy
578 downstream of JNK signaling. J Cell Sci. 2013;126(Pt 4):927-38.
579 41. Doggett K, Turkel N, Willoughby LF, Ellul J, Murray MJ, Richardson HE, et al. BTB-Zinc Finger
580 Oncogenes Are Required for Ras and Notch-Driven Tumorigenesis in Drosophila. PLoS One.
581 2015;10(7):e0132987.
582 42. Wu C, Ding X, Li Z, Huang Y, Xu Q, Zou R, et al. CtBP modulates Snail-mediated tumor invasion in
583 Drosophila. Cell Death Discov. 2021;7(1):202.

584 43. Jiang J, Kosman D, Ip YT, Levine M. The dorsal morphogen gradient regulates the mesoderm
585 determinant twist in early Drosophila embryos. Genes Dev. 1991;5(10):1881-91.
586 44. Ip YT, Park RE, Kosman D, Yazdanbakhsh K, Levine M. dorsal-twist interactions establish snail
587 expression in the presumptive mesoderm of the Drosophila embryo. Genes Dev. 1992;6(8):1518-30.
588 45. Stathopoulos A, Levine M. Whole-genome analysis of Drosophila gastrulation. Curr Opin Genet
589 Dev. 2004;14(5):477-84.
590 46. Hong JW, Hendrix DA, Papatsenko D, Levine MS. How the Dorsal gradient works: insights from
591 postgenome technologies. Proc Natl Acad Sci U S A. 2008;105(51):20072-6.
592 47. Jayawant E, Pack A, Clark H, Kennedy E, Ghodke A, Jones J, et al. NF-kappaB fingerprinting
593 reveals heterogeneous NF-kappaB composition in diffuse large B-cell lymphoma. Front Oncol.
594 2023;13:1181660.
595 48. Siddiqui I, Erreni M, Kamal MA, Porta C, Marchesi F, Pesce S, et al. Differential role of
596 Interleukin-1 and Interleukin-6 in K-Ras-driven pancreatic carcinoma undergoing mesenchymal
597 transition. Oncoimmunology. 2018;7(2):e1388485.
598 49. Treisman JE. Retinal differentiation in Drosophila. Wiley Interdiscip Rev Dev Biol. 2013;2(4):545-
599 57.
600 50. Newsome TP, Asling B, Dickson BJ. Analysis of Drosophila photoreceptor axon guidance in eye-
601 specific mosaics. Development. 2000;127(4):851-60.
602 51. Wu M, Pastor-Pareja JC, Xu T. Interaction between Ras(V12) and scribbled clones induces
603 tumour growth and invasion. Nature. 2010;463(7280):545-8.
604 52. Schindelin J, Arganda-Carreras I, Frise E, Kaynig V, Longair M, Pietzsch T, et al. Fiji: an open-
605 source platform for biological-image analysis. Nat Methods. 2012;9(7):676-82.

606

607

608

609

610

611

612

613

614

615

Figure legends

Fig 1. Extracellular and intracellular Toll signaling components contributes to *Ras^{V12}; scrib$^{-/-}$* tumour growth.

(A) A transcriptomics analysis comparing the profile of *Ras^{V12}; scrib$^{-/-}$* tumour cells to *GMR>GFP* control cells in the eye-antennal disc (EAD) identified 364 genes that are upregulated in the tumours. Among them, *PGRP-SA*, *GNBP2*, *easter*, *spz3* and *spz5* are genes taking part in the extracellular machinery leading to Toll pathway activation. PGRP-SA is highlighted in green because it is also found upregulated in two other tumour models. (B) Simplified version of Toll pathway activation upon bacterial infection. PGRP-SA (Peptidoglycan recognition protein SA) is a carboxypeptidase which recognizes and binds to peptidoglycans upon bacterial infection. Follows the formation of a trimeric complex together with a member of the GNBP family (Gram Negative Binding Protein) and the serine protease (ModSP). This complex initiates a multi-step proteolytic cascade that ultimately leads to the cleavage and activation of the ligand Spz. After the binding of Spz to the Toll receptor, the pathway is activated intracellularly through the activation and formation of a complex composed of the adaptor proteins Myd88 and Tube as well as the serine-threonine protein kinase Pelle. Pelle subsequently phosphorylates the inhibitor cactus, the homolog of mammalian IkappaB, which is targeted to proteasome degradation. As Cactus sequesters the NF-kB Dorsal into the cytoplasm, its degradation triggers the translocation of Dorsal into the nucleus and the transcription of its target genes. (C) Cartoon of the genetic setting used in this study for manipulating *Ras^{V12}; scrib$^{-/-}$* tumours. GFP-labelled tumours are generated from randomly-selected single epithelial cells from the EAD. They grow and fuse to form large tumours that start invading the central nervous system (CNS) through the Optic Lobe (OL) first and the Ventral Nerve Cord (VNC) later. Tumour cells also sometimes reach the leg discs (LD). (D) Representative confocal pictures and quantifications of the mean tumour volumes of GFP-labelled control tumours (n=21, m=3,71x10^7 µm^3, SD=±0,47x10^7 µm^3) and *PGRP-SA Ras^{V12}; scrib$^{-/-}$* tumours (n=17, m=2,11x10^7 µm^3, SD=±0,19x10^7 µm^3) at day8 after egg laying, statistical significance was determined with an unpaired T-test with Welch's correction. (E) Representative confocal pictures and quantifications of the mean tumour volumes of GFP-labelled control (n=20, m=8,46x10^7 µm^3, SD=±1,77,53x10^7 µm^3) and *ModSP^{IR} Ras^{V12}; scrib$^{-/-}$ Dcr2* tumours (n=30, m=5,07x10^7 µm^3, SD=±1,00x10^7 µm^3) at Day8 (29°C), statistical significance was determined with an unpaired T-test with Welch's correction. (F) Representative confocal pictures and quantifications of the mean tumour volumes of GFP-labelled control tumours (n=10, m=2,64x10^7 µm^3, SD=±0,76x10^7 µm^3) and *pelle^{IR} Ras^{V12}; scrib$^{-/-}$* tumours (n=10, m=0,78x10^7 µm^3, SD=±0,22x10^7 µm^3) at Day6 (29°C), statistical significance was determined with a Mann-Whitney test. Scale bars=50µm.

Fig 2. Two splicing variants of the NF-kB Dorsal are aberrantly expressed in *Ras^{V12}*-driven tumours.

(A) Immunostainings against Dorsal-A (DlA in green) and Dorsal-B (DlB in magenta) in BFP-labelled *wt* clones (n=20 EADs), *scrib^{IR}* tumours (n=23 EADs), *Ras^{V12}* tumours (n=20 EADs) and *Ras^{V12}; scrib^{IR}* tumours (n=24 EADs) at day 6. DlA and DlB accumulation is observed only in *Ras^{V12}*-driven tumours and appears mainly mutually exclusive. (B) Immunostaining against DlA

659 (green) and DlB (magenta) in BFP-labelled *Ras^{V12}; scrib^{IR}* tumours (white) (n=24 EADs) and
660 close-ups showing that DlA and DlB are not expressed in the same subset of cells. Colocalization
661 analysis assessed with the Pearson's correlation coefficient reveals a poor colocalization between
662 DlA and DlB in the tumours (n=24, m=0,11, SD=±0,08). (C) Heat map of DlA intensity within a
663 representative BFP-labelled *Ras^{V12}; scrib^{IR}* tumour-bearing EAD at day 6. The tumour is outlined
664 with the straight white line. An arbitrary intensity threshold set at 250 (gray line on the graph)
665 allows the clear segregation of a DlAhigh ("tumour High") and a DlAlow ("tumour Low") cell
666 population within the tumour. Quantifications of the mean DlA intensity of the "tumour High" (n=23,
667 m=458,7, SD=±28,4), "tumour Low" (n=23, m=135,2, SD=±7,0) and wt Tumour microenvironment
668 (TME) (n=23, m=82,2, SD=±6,7) demonstrates a general elevation of DlA levels within the tumour
669 compared to wt cells. Statistical significance was determined with a Tukey's multiple comparison
670 test. (D) Heat map of DlB intensity within a representative RasV12; scribIR tumour-bearing EAD
671 at day 6. The tumour is outlined with the straight white line. An arbitrary intensity threshold set at
672 10000 (gray line on the graph) allows the clear segregation of a DlBhigh ("tumour High") and a
673 DlBlow ("tumour Low") cell population within the tumour. Quantifications of the mean DlB intensity
674 of the "tumour High" (n=24, m=20331,9, SD=±3108,7), "tumour Low" (n=24, m=3955,8,
675 SD=±584,5) and wt Tumour microenvironment (TME) (n=23, m=4660,9, SD=±1187,3).
676 Normalization was done by subtracting the background intensity. Statistical significance was
677 determined with a Dunn's multiple comparison test. Scale bars=20µm.

678

679 **Fig 3. Cell type-dependent Dorsal isoforms accumulation correlates with tumour**
680 **neurogenesis and apoptosis.**

681 (A) Representative confocal pictures of BFP-labelled *Ras^{V12}; scrib^{IR}* tumours, expressing the a
682 DlA::GFP fusion protein at endogenous levels (green), overtime (Day 4 n=18 EADs, Day 5 n= 14
683 EADs, Day 6 n=18 EADs, Day 7 n= 17 EADs, Day 8 n=20 EADs and Day 9 n=11 EADs) stained
684 for the pan-neuronal marker Elav (magenta). The cephalic complex is outlined with the straight
685 gray line and the tumour is outlined with the straight white line on the close-ups. Yellow arrows
686 points at neurons that are negative for DlA. Scale bar=50µm. (B) Representative confocal pictures
687 of GFP-labelled *cherry^{IR} Ras^{V12}; scrib^{IR}* (n=8 EADs) at day 6 (29°C) stained for Elav (green) and
688 DlA (magenta). The tumour is outlined with the straight white line. DlA and Elav appears mutually
689 exclusive. Scale bar=20µm. (C) Representative confocal pictures of GFP-labelled *cherry^{IR}*
690 *Ras^{V12}; scrib^{IR}* (n=8 EADs) at day 6 (29°C) stained for Elav (green) and DlB (magenta). The
691 tumour is outlined with the straight white line. DlB and Elav are expressed in the same tumour
692 cells. Scale bar=20µm. (D) Representative confocal pictures of GFP-labelled *cherry^{IR} Ras^{V12};*
693 *scrib^{IR}* control tumours (n=62 EADs) at day 6 (29°C) stained for Elav (green) and cDcp1 (magenta).
694 The tumour is outlined with the straight white line. cDcp1^{+} cells are mostly found in areas of the
695 tumour where neurons are present where we often observe neuron apoptosis (yellow arrows).
696 Scale bar=20µm. (E) Representative confocal pictures of GFP-labelled *Ras^{V12}; scrib^{IR}* control
697 tumours (n=7 EADs) and *Diap1^{OE} Ras^{V12}; scrib^{IR}* (n=9 EADs) stained for cDcp1 (magenta) at day
698 6. Scale bar=50µm. (F) Representative confocal pictures of GFP-labelled *Ras^{V12}; scrib^{IR}* control
699 tumours (n=13 EADs) and *Diap1^{OE} Ras^{V12}; scrib^{IR}* (n=7 EADs) stained for DlA (green) and DlB
700 (magenta) at day 6. Scale bar=20µm.

701

702 **Fig 4. Dorsal represses *Ras^{V12} scrib^{RNAi}* tumour differentiation and apoptosis.**

703 (A) Representative confocal pictures and quantifications of the mean tumour volumes of GFP-
704 labelled *Cherry^{IR} Ras^{V12}; scrib^{IR}* control tumours (n=36, m=8,32x10^{7}µm^3, SD=±1,31 x10^{7}µm^3),
705 *dorsal^{IR-1} Ras^{V12}; scrib^{IR}* tumours (n=25, m=1,97x10^{7}µm^3, SD=± 1,00x10^{7}µm^3), *Cherry^{IR} Ras^{V12};*
706 *scrib^{IR} Dcr2* control tumours (n=43, m=8,52x10^{7}µm^3, SD=±1,64x10^{7}µm^3) and *dorsal^{IR-2} Ras^{V12};*
707 *scrib^{IR} Dcr2* tumours (n=37, m=4,71x10^{7}µm^3, SD=±1,85x10^{7}µm^3) at Day12 (29°C), statistical
708 significance was determined with an unpaired T-test with Welch's correction. Scale bar=50µm.
709 (B) Representative confocal pictures and quantifications of the proliferation ratio of GFP-labelled
710 *Cherry^{IR} Ras^{V12}; scrib^{IR}* control tumours (n=36, m=1,08%, SD=±0,41%) and *dorsal^{IR-1} Ras^{V12};*
711 *scrib^{IR}* tumours (n=35, m=1,39%, SD=±0,83%) at Day8 (29°C). Proliferation was detected through
712 immunostainings against the mitotic marker pH3 (phospho-Histone 3, in magenta). Here, the
713 proliferation ratio is defined as the ratio between the pH3 area within the tumour and the area of
714 the tumour itself. Scale bar=20µm. (C) Representative confocal pictures and quantifications of the
715 differentiation ratio of GFP-labelled *Cherry^{IR} Ras^{V12}; scrib^{IR}* control tumours (n=63, m=8,29%,
716 SD=±2,87%) and *dorsal^{IR-1} Ras^{V12}; scrib^{IR}* tumours (n=57, m=24,40%, SD=±7,09%) at Day8
717 (29°C). Differentiation was detected through immunostainings against the pan-neuronal marker
718 Elav (magenta). Here, the differentiation ratio is defined as the ratio between the Elav area within
719 the tumour and the area of the tumour itself. Scale bar=20µm. (D) Representative confocal
720 pictures and quantifications of the apoptosis ratio of GFP-labelled *Cherry^{IR} Ras^{V12}; scrib^{IR}* control
721 tumours (n=63, m=0,71%, SD=±0,29%) and *dorsal^{IR-1} Ras^{V12}; scrib^{IR}* tumours (n=57, m=1,45%,
722 SD=±0,46%) at Day8 (29°C). Apoptosis was detected through immunostainings against the
723 cleaved effector caspase, cDcp1 (cleaved-Death Caspase 1, in magenta). Here, the apoptosis
724 ratio is defined as the ratio between the cDcp1 area within the tumour and the area of the tumour
725 itself. Statistical significance was determined with an unpaired T-test with Welch's correction.
726 Scale bar=20µm.

727 **Fig 5. Dorsal amplifies JNK signaling**

728 (A) Representative confocal pictures of BFP-labelled *Ras^{V12}; scrib^{IR}* tumours, expressing the JNK
729 activity reporter, TRE-eGFP (green) and stained for DIA (magenta). The tumour is outlined with
730 the straight white line. Colocalization analysis assessed with the Pearson's correlation coefficient
731 reveals a weak colocalization between DIA and JNK activity in the tumours (n=31, m=0,23,
732 SD=±0,08). Scale bar=20µm. (B) Representative confocal pictures of GFP-labelled *cherry^{IR}*
733 *Ras^{V12}; scrib^{IR}* tumours stained for pJNK (green) and DIB (magenta) at day6 (29°C). The tumour
734 is outlined with the straight white line. Colocalization analysis assessed with the Pearson's
735 correlation coefficient reveals a good colocalization between DIB and pJNK in the tumours (n=25,
736 m=0,41, SD=±0,06). Scale bar=20µm. (C) Representative confocal pictures and quantifications
737 of the mean MMP1 intensity of GFP-labelled *Ras^{V12}; scrib^{IR}* tumours (n=11, m=1,00, SD=±0,06),
738 *dorsal^{OE} Ras^{V12}; scrib^{IR}* tumours (n=11, m=2,85, SD=0,57) and *modSP^{OE} Ras^{V12}; scrib^{IR}* tumours
739 (n=10, m=1,49, SD=±0,32) at day 6. Intensity normalization was done by subtracting the
740 background intensity on each picture and finally dividing each data point by the mean intensity
741 value for the control tumours for each replicate. Statistical significance was determined with
742 Dunnett's T3 multiple comparisons test. Scale bars=50µm.

743 **Fig 6. Dorsal stimulates tumour migration and the Dorsal targets Snail and Twist contribute**
744 **to tumour growth**

745 (A) Z-projections of representative confocal pictures of size-matched GFP-labelled *Cherry^{IR}*
746 *Ras^{V12}; scrib^{IR}* tumours (n=3 EADs) and *dorsal^{IR-1} Ras^{V12}; scrib^{IR}* tumours (n=8 EADs) at day 12
747 (29°C), stained for Hoechst (magenta). Scale bars=50µm. The cephalic complexes (and leg discs

748 on the small inserts) are outlined with the straight gray line. A cartoon represents the three
749 invasion parameters assessed in this study: the VNC (Ventral Nerve Cord) invasion score, ranged
750 between c and 1, is greater the further tumour cells migrate toward the tip of the VNC (green
751 arrow), indicated as "VNC=" on the Z-projection images; the frequency of leg discs invasion (small
752 insert with leg discs confocal pictures, Scale bars=20µm) and the fusion of distinct EAD (Eye-
753 Antennal Disc) tumours (white arrow, dashed line indicates the visible separation of both neighbor
754 EADs). For the VNC score, statistical significance was determined with Dunnett's T3 multiple
755 comparisons test. (B) Z-projections of representative confocal pictures of GFP-labelled and
756 *Ras^{V12}; scrib^{IR}* (n=15 EADs) and *dorsal^{OE} Ras^{V12}; scrib^{IR}* tumours (n=24 EADs) at day 6, stained
757 for Hoechst (magenta). The cephalic complexes (and leg discs on the small inserts) are outlined
758 with the straight gray line. Quantification of the mean tumour volumes of GFP-labelled *Ras^{V12};*
759 *scrib^{IR}* (n=9, m=9,71x10^{6}µm^3, SD=±1,53x10^{6}µm^3) and *dorsal^{OE} Ras^{V12}; scrib^{IR}* tumours (n=11,
760 m=6,52x10^{6}µm^3, SD=±1,12x10^{6}µm^3) at day 6. OL: Optic Lobe. Statistical significance was
761 determined with an unpaired T-test with Welch's correction. Scale bars=50µm. (C) Representative
762 confocal pictures and quantification the mean tumour volume of GFP-labelled *cherry^{IR} Ras^{V12};*
763 *scrib^{IR}* (n=12, m=4,83x10^{5}µm^3, SD=±1,52x10^{5}µm^3), and *snail^{IR} Ras^{V12}; scrib^{IR}* (n=9,
764 m=1,41x10^{5}µm^3, SD=±0,65 x10^{5}µm^3). Statistical significance was determined with a Mann
765 Whitney's test. (D) Representative confocal pictures and quantification the mean tumour volume
766 of GFP-labelled *cherry^{IR} Ras^{V12}; scrib^{IR}* (n=20, m=7,17x10^{7}µm^3, SD=±1,22x10^{7}µm^3) and *twist^{IR-1}*
767 *Ras^{V12}; scrib^{IR}* (n=7, m=1,81x10^{7}µm^3, SD=±0,83x10^{7}µm^3) as well as *Cherry^{IR} Ras^{V12}; scrib^{IR} Dcr2*
768 control tumours (n=24, m=6,89x10^{7}µm^3, SD=±1,12x10^{7}µm^3) and twist^{IR-2} *Ras^{V12}; scrib^{IR} Dcr2*
769 tumours (n=13, m=3,98x10^{7}µm^3, SD=±1,43x10^{7}µm^3). VNC invasion scores are indicated.
770 Statistical significance was determined with a Mann Whitney's test. Scale bars=50µm.

771 **Fig 7. Working Model**

772 In this working model, we propose that the protein level of the NF-kB Dorsal regulate different
773 aspect of tumorigenesis. Invasion: In the most posterior part of the tumour, high levels of Dorsal
774 promote invasion of the tumour cells in the adjacent organs through elevation of JNK signaling
775 and the EMT transcription factor Snail and Twist that would promote cytoskeleton remodelling.
776 Tumour growth: In the rest of the tumour where more intermediate levels of Dorsal are observed,
777 Dorsal would stimulate tumour growth by repressing differentiation and apoptosis. Regulation: At
778 least two factors seem two trigger aberrant level of Dorsal within the tumours. Genetically, Ras^{V12}
779 make tumour cells competent to accumulate higher levels of Dorsal throughout the entire tumour.
780 Locally, a spatiotemporal control is exerted at the posterior part of the tumour where neurons are
781 formed, to reach very high levels of Dorsal. A possibility is an increase local Toll pathway
782 activation triggered by high Spz concentration from the brain which will promote Dorsal expression.
783 There, we observe alternative splicing of DlA versus DlB which segregate in different tumour
784 subpopulations. We hypothesize that the heterogeneity in Dorsal isoforms and/or levels promote
785 a balance between tumour growth and invasion favoring tumorigenesis.

786 **S1 Fig. Localization of DlA, DlB and Cactus.**

787 (A) Representative confocal pictures of GFP-labelled *Ras^{V12}; scrib$^{-/-}$* tumours (n=10 EADs) at day
788 6, generated with the conventional EyMARCM genetic system and stained for DlA (magenta) and
789 Hoechst (blue). Consistent with the data generated with our new EyaHost genetic system in Fig
790 2, DlA levels are aberrant in the tumours. The tumour is outlined with a straight white line. Scale
791 bars=50µm. (B) Representative confocal pictures of GFP-labelled *Ras^{V12}; scrib^{IR}* tumours at day
792 6, generated with our novel EyaHost genetic system and stained for DlA (green), DlB (magenta)

793 and Hoechst (blue). The tumour cells that already migrated inside the optic lobe (OL) of the CNS
794 express high levels of DlA or DlB, suggesting their potential involvement in tumour cell migration.
795 Scale bars=50µm. (C) Representative confocal pictures of BFP-labelled *genomic-cactus::GFP,*
796 *Ras^{V12}; scrib^{IR}* tumours stained for DlB (magenta) at day 6 (upper line) (n=6 EADs) or stained for
797 DlA (magenta) at day 8 (lower line) (n=6 EADs). The tumour is outlined with a straight white line.
798 Scale bars=20µm.

799

800 **S2 Fig. The endogenous Dl reporter used in this study is a DlA specific reporter.**

801 (A) Representative confocal pictures of BFP-labelled *genomic-dorsal::GFP Ras^{V12}; scrib^{IR}*
802 tumours at day 6, stained for DlA (magenta) and DlB (blue). The tumour is outlined with the
803 straight white line. Scale bars=50µm. (B) Colocalization analyses assessed with the Pearson's
804 correlation coefficient reveal a good colocalization between DlA and Dorsal::GFP (n=24, m=0,44,
805 SD=±0,06) and no colocalization between DlB and Dorsal::GFP in the tumours (n=24, m=0,09,
806 SD=±0,07) suggesting that this reporter is a DlA specific fusion protein. Statistical significance
807 was determined with an unpaired T-test with Welch's correction.

808 **S3 Fig. Dorsal knockdown efficiencies and pelle knockdown mimicks the function of**
809 **Dorsal on differentiation and survival.**

810 (A) Representative confocal pictures and quantification of the mean DlA intensity of GFP-labelled
811 *cherry^{IR} Ras^{V12}; scrib^{IR}* (n=6, m=1,00, SD=±0,14) and *dorsal^{IR-1} Ras^{V12}; scrib^{IR}* tumours (n=6,
812 m=0,54, SD=±0,03) as well as *Cherry^{IR} Ras^{V12}; scrib^{IR} Dcr2* control tumours (n=5, m=1,00,
813 SD=±0,14) and *dorsal^{IR-2} Ras^{V12}; scrib^{IR} Dcr2* tumours (n=6, m=0,32, SD=±0,05) at day 6 (29°C).
814 Intensity normalization was done by subtracting the background intensity on each picture and
815 finally dividing each data point by the mean intensity value for the control tumours for each
816 replicate. Statistical significance was determined with a Mann-Whitney test. Scale bars=20µm.
817 (B) Representative confocal pictures and quantification of the mean DlB intensity of GFP-labelled
818 *cherry^{IR} Ras^{V12}; scrib^{IR}* (n=7, m=1,00, SD=±0.19) and *dorsal^{IR-1} Ras^{V12}; scrib^{IR}* tumours (n=9,
819 m=0.40, SD=±0.12) as well as *Cherry^{IR} Ras^{V12}; scrib^{IR} Dcr2* control tumours (n=5, m=1.00,
820 SD=±0.31) and *dorsal^{IR-2} Ras^{V12}; scrib^{IR} Dcr2* tumours (n=6, m=0.54, SD=±0.15) at day 6 (29°C).
821 Intensity normalization was done by subtracting the background intensity on each picture and
822 finally dividing each data point by the mean intensity value for the control tumours for each
823 replicate. Statistical significance was determined with a Mann-Whitney test. Scale bars=20µm.
824 (C) Z-projection of representative confocal pictures of GFP-labelled *RFP^{IR} Ras^{V12}; scrib^{IR}* control
825 tumours and *pelle^{IR} Ras^{V12}; scrib^{IR}* tumours at day 6 (29°C), stained for Elav (green) and cDcp1
826 (magenta). The tumour is outlined with a straight white line. Quantification of the apoptosis ratio
827 of *RFP^{IR} Ras^{V12}; scrib^{IR}* control tumours (n=16, m=4,97%, SD=±2,23%) and *pelle^{IR} Ras^{V12}; scrib^{IR}*
828 tumours (n=15, m=17,84%, SD=±4,16%) at day 6 (29°C). Here, the apoptosis ratio is defined as
829 the ratio between the cDcp1 area within the tumour and the area of the tumour itself. Statistical
830 significance was determined with an unpaired T-test with Welch's correction. Quantification of the
831 differentiation ratio of *RFP^{IR} Ras^{V12}; scrib^{IR}* control tumours (n=5, m=18,04%, SD=±5,99%) and
832 *pelle^{IR} Ras^{V12}; scrib^{IR}* tumours (n=8, m=44,14%, SD=±8,83%) at day 6 (29°C). Here, the
833 differentiation ratio is defined as the ratio between the Elav area within the tumour and the area
834 of the tumour itself. Statistical significance was determined with a Mann-Whitney test. Scale
835 bars=50µm.

836 **S4 Fig. Dorsal is sufficient to induce dysplasia and delamination but not overgrowth and**
837 **invasion.**

838 (A) Representative confocal pictures and quantification of the mean clone volume of GFP-labelled
839 *wt* clones (n=20, m=5,59x10^5µm^3, SD=±0,69x10^5µm^3) and *dorsal*^{OE} clones (n=30,
840 m=4,87x10^5µm^3, SD=±0,66x10^5µm^3) at day 6, stained for DlA (magenta) and Hoechst (blue).
841 Displasic clones are observed in 100% of the *dorsal*^{OE} clones-bearing EADs. GFP-labelled cells
842 are never found in the VNC as indicated with the VNC score values. Scale bars=50µm. (B)
843 Reconstruction of an orthogonal view of *wt* clones and *dorsal*^{OE} clones representing the EAD
844 tissue (magenta) and the GFP-labelled clones (green). GFP-labelled cells extend from the apical
845 to the basal side of the pseudostratified epithelium of the EAD of *wt* clones whereas some
846 *Dorsal*^{OE} clones spread basally (yellow arrow).

847

848

849

850

851

852

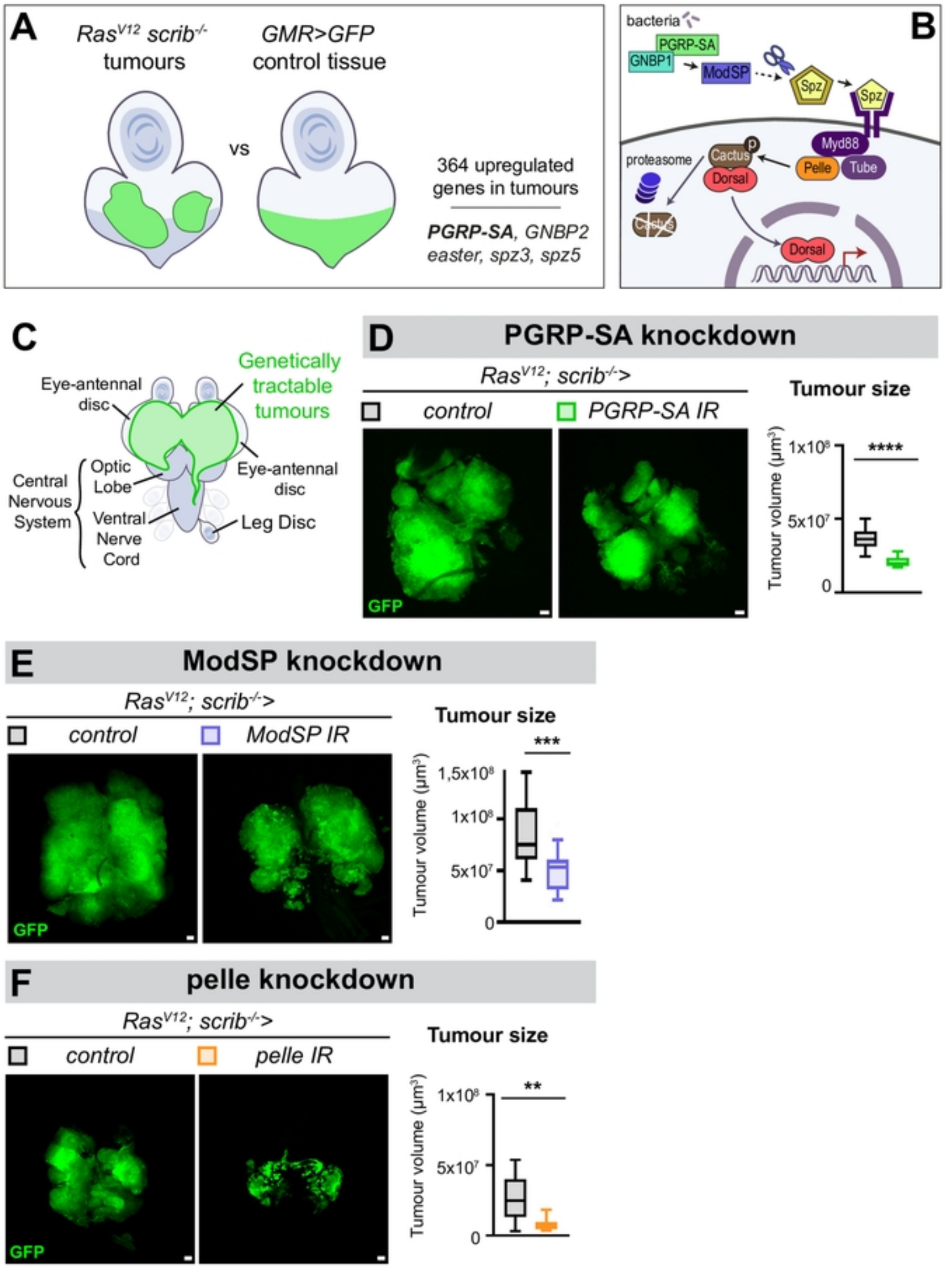
A
Ras^{V12} scrib$^{-/-}$ tumours
GMR>GFP control tissue
vs
364 upregulated genes in tumours
PGRP-SA, GNBP2
easter, spz3, spz5
B
bacteria
PGRP-SA
GNBP1
ModSP
Spz
Spz
Myd88
proteasome
Cactus
p
Dorsal
Pelle
Tube
Cactus
Dorsal
C
Genetically tractable tumours
Eye-antennal disc
Eye-antennal disc
Central Nervous System
Optic Lobe
Ventral Nerve Cord
Leg Disc
D
PGRP-SA knockdown
Ras^{V12}; scrib$^{-/-}$>
control
PGRP-SA IR
GFP
Tumour size
Tumour volume (µm^3)
1x10^8
5x10^7
0
****
E
ModSP knockdown
Ras^{V12}; scrib$^{-/-}$>
control
ModSP IR
GFP
Tumour size
Tumour volume (µm^3)
1,5x10^8
1x10^8
5x10^7
0
***
F
pelle knockdown
Ras^{V12}; scrib$^{-/-}$>
control
pelle IR
GFP
Tumour size
Tumour volume (µm^3)
1x10^8
5x10^7
0
**

Figure

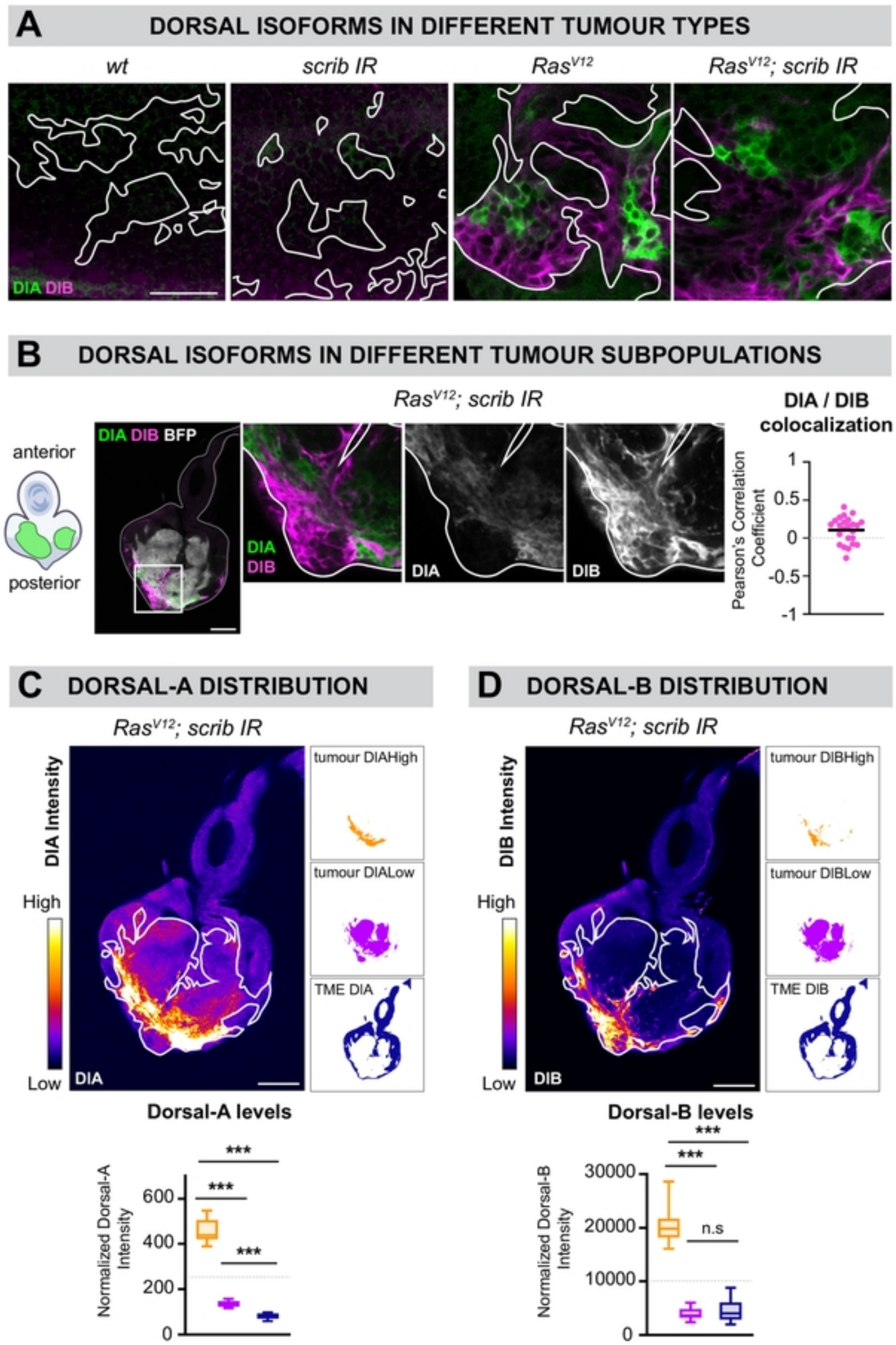
A
DORSAL ISOFORMS IN DIFFERENT TUMOUR TYPES
wt
scrib IR
Ras^{V12}
Ras^{V12}; scrib IR
DIA DIB
B
DORSAL ISOFORMS IN DIFFERENT TUMOUR SUBPOPULATIONS
Ras^{V12}; scrib IR
DIA / DIB colocalization
anterior
posterior
DIA DIB BFP
DIA
DIB
DIA
DIB
Pearson's Correlation Coefficient
1
0.5
0
-0.5
-1
C
DORSAL-A DISTRIBUTION
Ras^{V12}; scrib IR
DIA Intensity
High
Low
DIA
tumour DIAHigh
tumour DIALow
TME DIA
Dorsal-A levels
Normalized Dorsal-A Intensity
600
400
200
0
***
***
***
D
DORSAL-B DISTRIBUTION
Ras^{V12}; scrib IR
DIB Intensity
High
Low
DIB
tumour DIBHigh
tumour DIBLow
TME DIB
Dorsal-B levels
Normalized Dorsal-B Intensity
30000
20000
10000
0
***
***
n.s

Figure

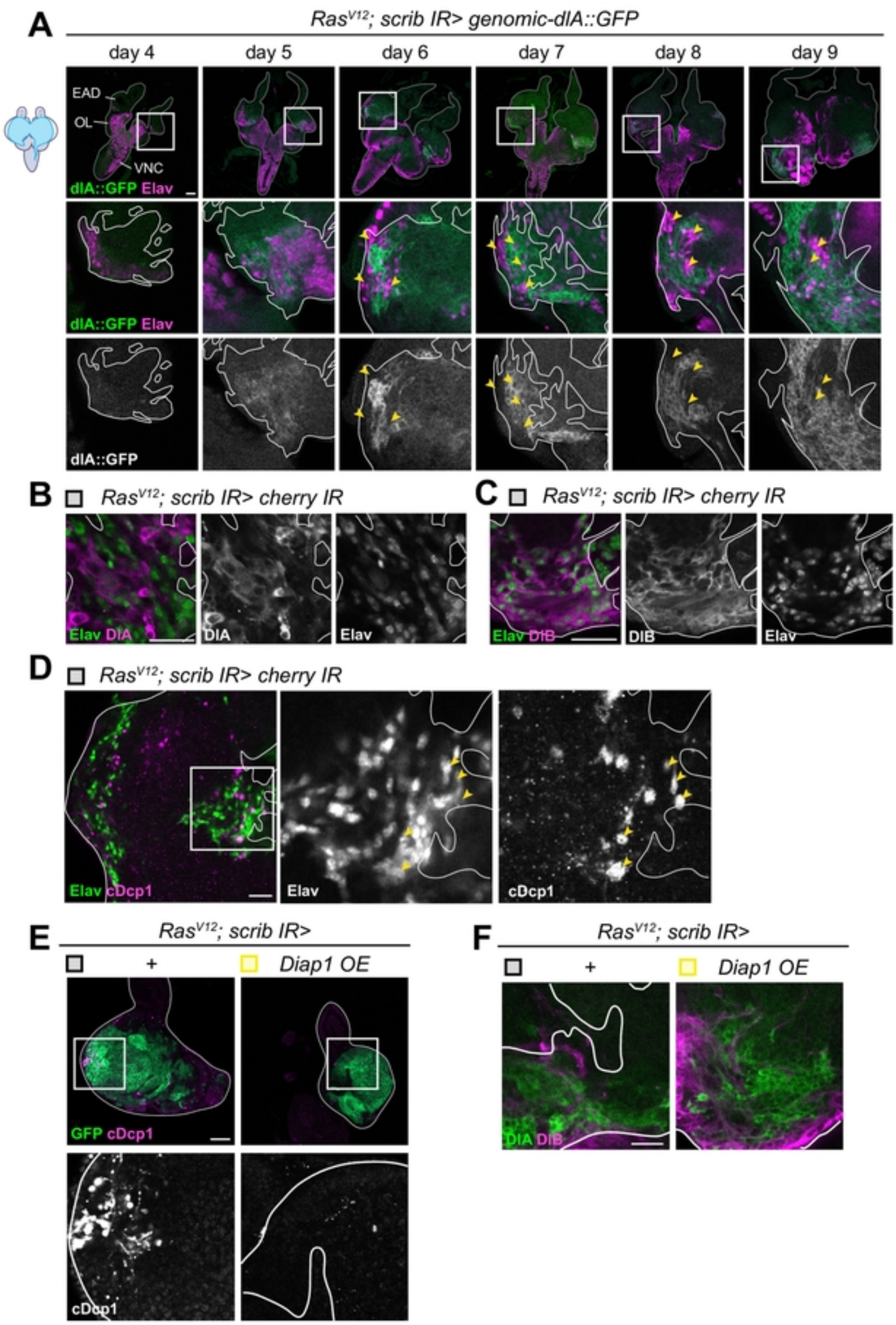
A
Ras^{V12}; scrib IR> genomic-dIA::GFP
day 4
day 5
day 6
day 7
day 8
day 9
EAD
OL
VNC
dIA::GFP Elav
dIA::GFP
B
Ras^{V12}; scrib IR> cherry IR
Elav DIA
DIA
Elav
C
Ras^{V12}; scrib IR> cherry IR
Elav DIB
DIB
Elav
D
Ras^{V12}; scrib IR> cherry IR
Elav cDcp1
Elav
cDcp1
E
Ras^{V12}; scrib IR>
+
Diap1 OE
GFP cDcp1
cDcp1
F
Ras^{V12}; scrib IR>
+
Diap1 OE
DIA DIB

Figure

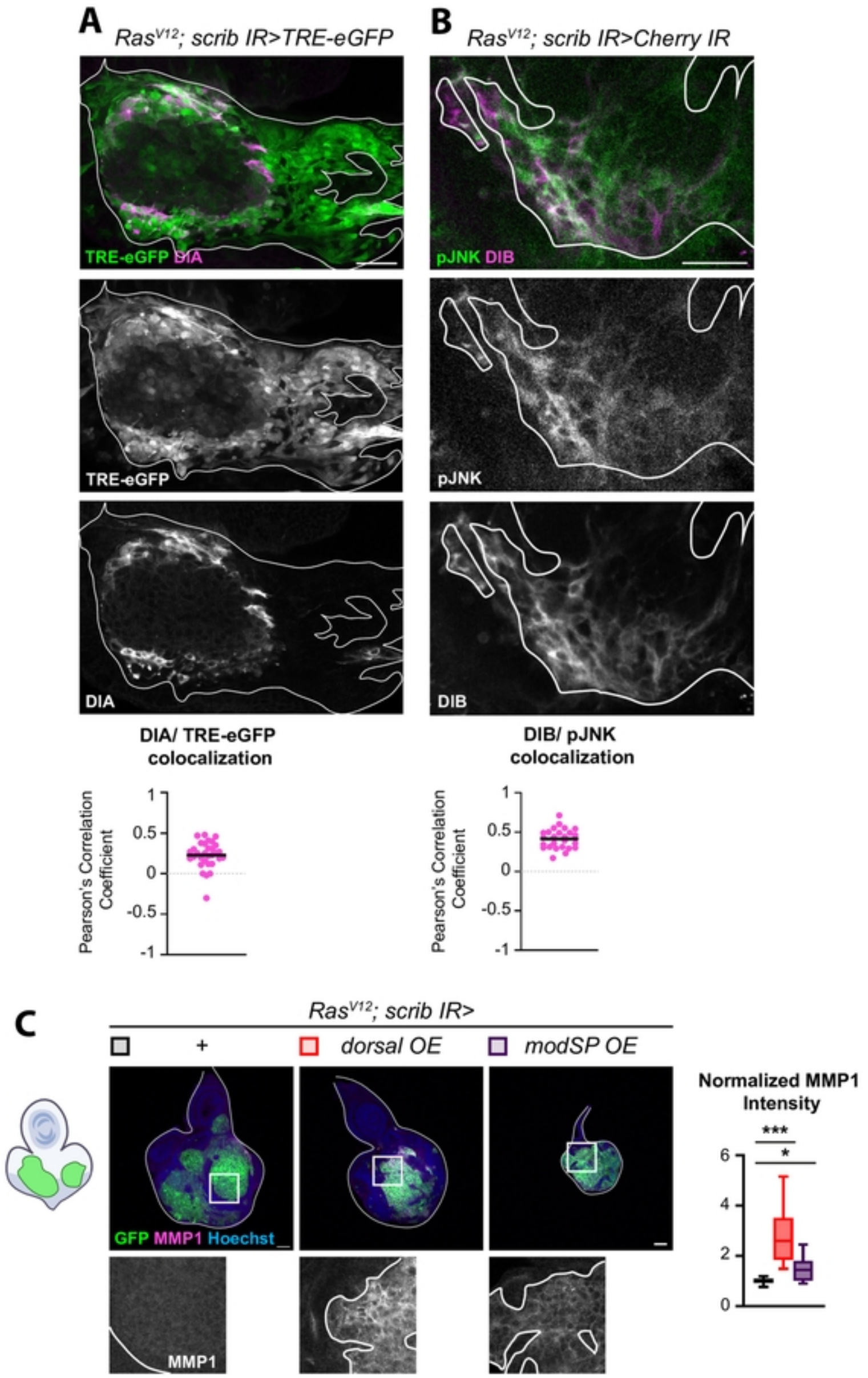
A
Ras^{V12}; scrib IR>TRE-eGFP
TRE-eGFP DIA
TRE-eGFP
DIA
B
Ras^{V12}; scrib IR>Cherry IR
pJNK DIB
pJNK
DIB
DIA/ TRE-eGFP colocalization
Pearson's Correlation Coefficient
1
0.5
0
-0.5
-1
DIB/ pJNK colocalization
Pearson's Correlation Coefficient
1
0.5
0
-0.5
-1
C
Ras^{V12}; scrib IR>
+
dorsal OE
modSP OE
GFP MMP1 Hoechst
MMP1
Normalized MMP1 Intensity
***
*
6
4
2
0

Figure

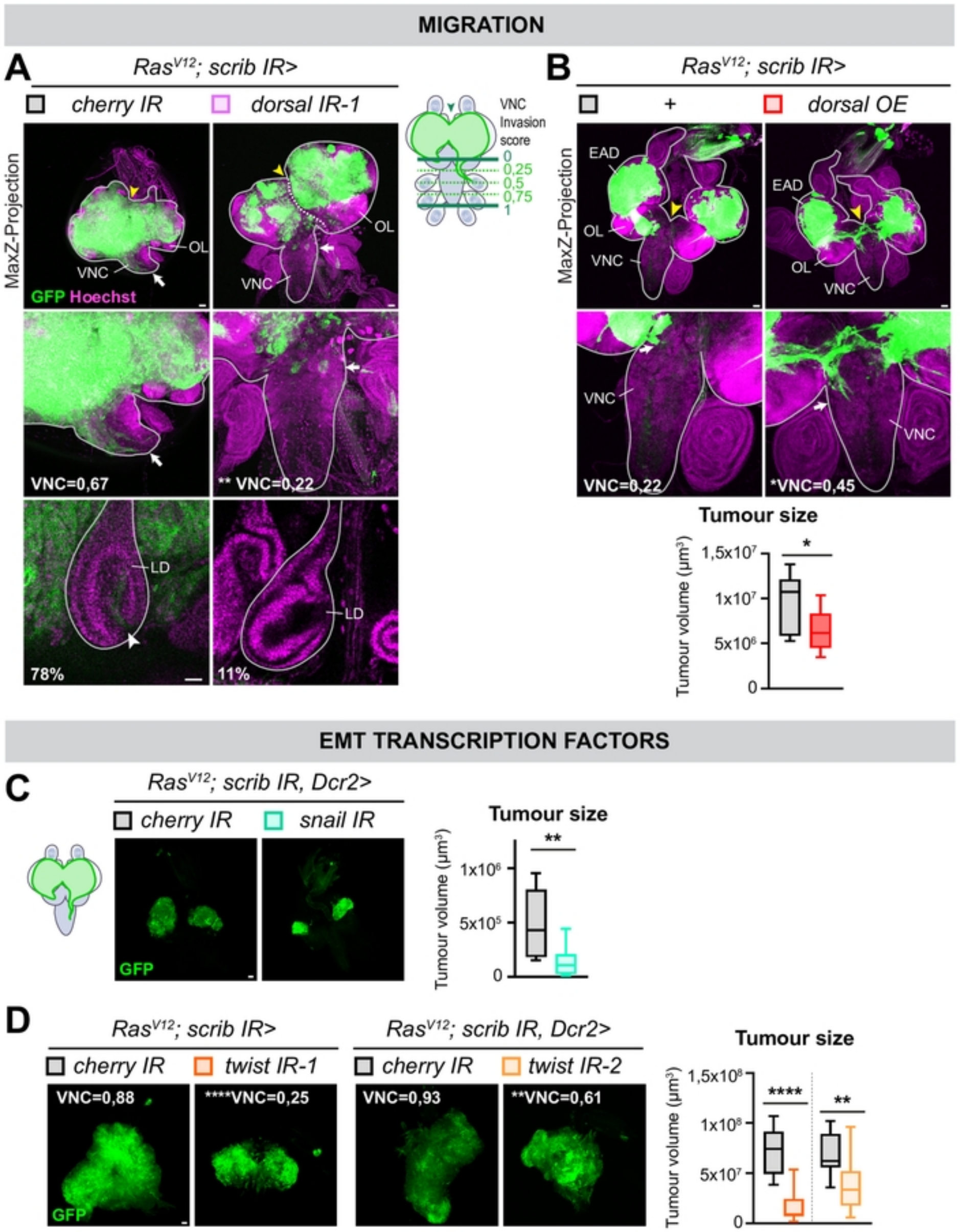
MIGRATION
A
Ras^{V12}; scrib IR>
cherry IR
dorsal IR-1
MaxZ-Projection
VNC
OL
GFP Hoechst
VNC=0,67
** VNC=0,22
LD
78%
11%
VNC
Invasion
score
0
0,25
0,5
0,75
1
B
Ras^{V12}; scrib IR>
+
dorsal OE
EAD
OL
VNC
VNC=0,22
*VNC=0,45
Tumour size
Tumour volume (µm³)
1,5x10⁷
1x10⁷
5x10⁶
0
*
EMT TRANSCRIPTION FACTORS
C
Ras^{V12}; scrib IR, Dcr2>
cherry IR
snail IR
GFP
Tumour size
Tumour volume (µm³)
1x10⁶
5x10⁵
0
**
D
Ras^{V12}; scrib IR>
cherry IR
twist IR-1
VNC=0,88
****VNC=0,25
Ras^{V12}; scrib IR, Dcr2>
cherry IR
twist IR-2
VNC=0,93
**VNC=0,61
GFP
Tumour size
Tumour volume (µm³)
1,5x10⁸
1x10⁸
5x10⁷
0
****
**

Figure

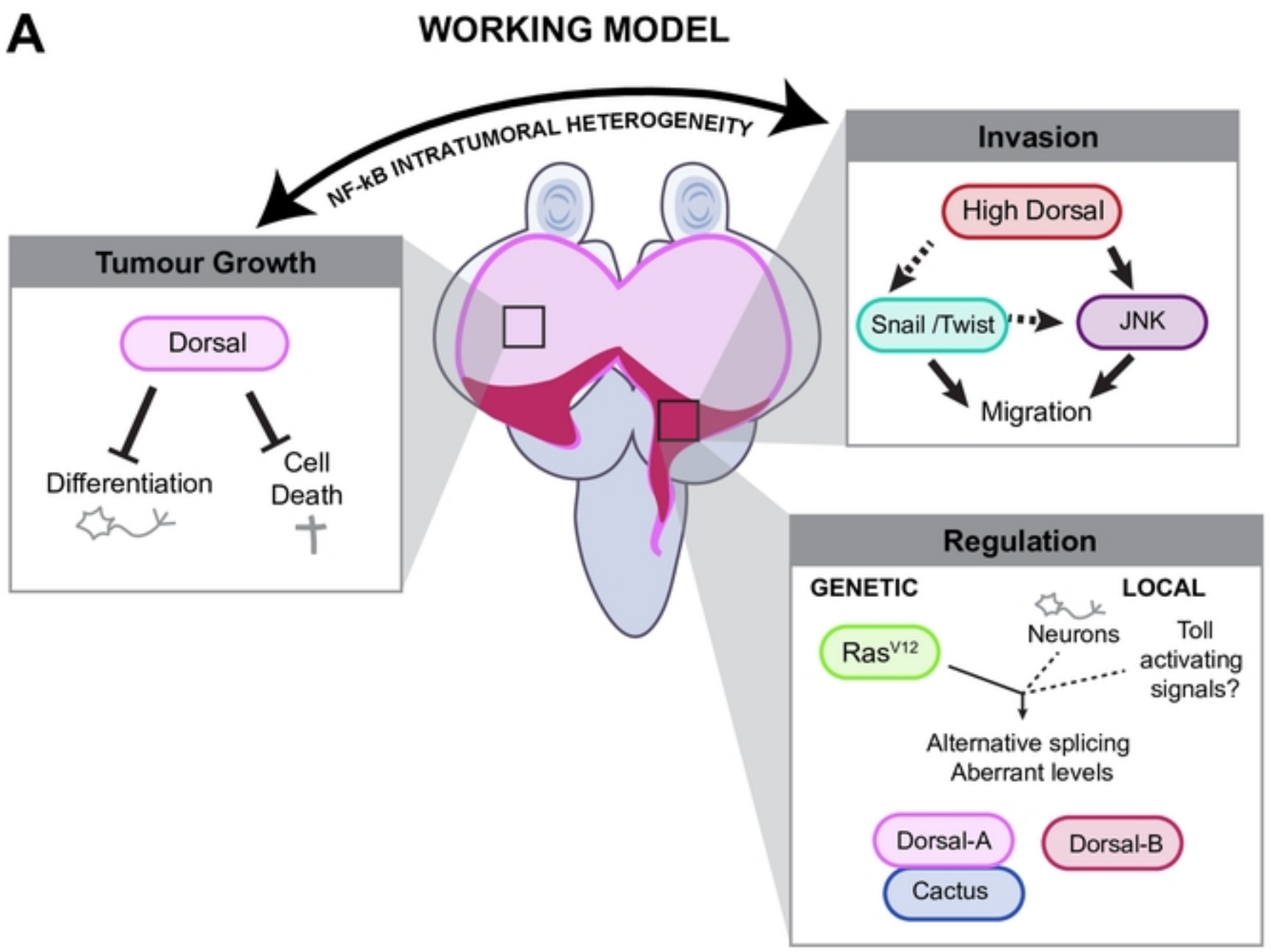
A
WORKING MODEL
NF-kB INTRATUMORAL HETEROGENEITY
Tumour Growth
Dorsal
Differentiation
Cell Death
Invasion
High Dorsal
Snail /Twist
JNK
Migration
Regulation
GENETIC
LOCAL
Ras^{V12}
Neurons
Toll activating signals?
Alternative splicing
Aberrant levels
Dorsal-A
Dorsal-B
Cactus

Figure

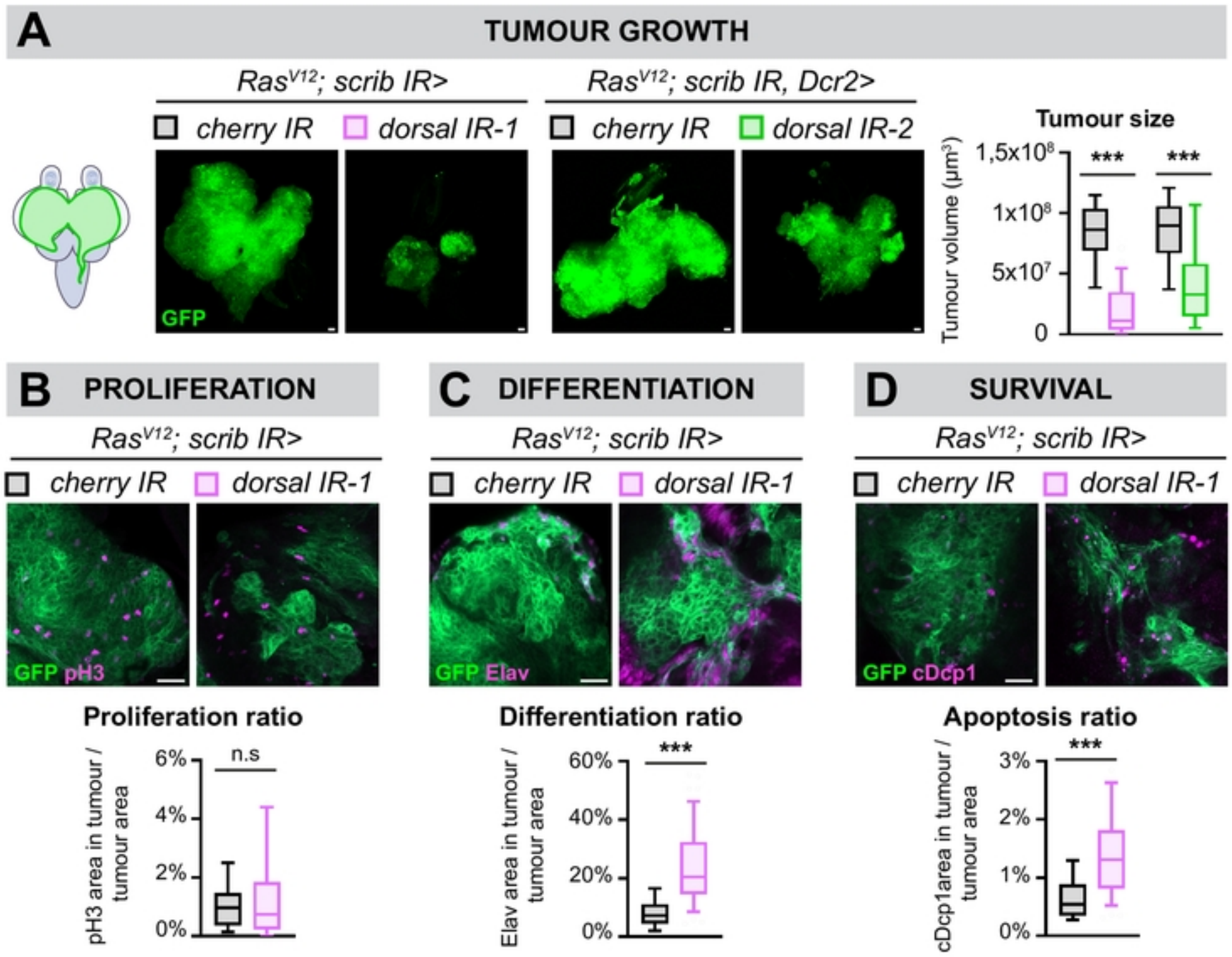
A
TUMOUR GROWTH
Ras^{V12}; scrib IR>
Ras^{V12}; scrib IR, Dcr2>
cherry IR
dorsal IR-1
cherry IR
dorsal IR-2
GFP
Tumour size
Tumour volume (µm³)
1,5x10⁸
1x10⁸
5x10⁷
0
***
***
B
PROLIFERATION
Ras^{V12}; scrib IR>
cherry IR
dorsal IR-1
GFP pH3
Proliferation ratio
pH3 area in tumour / tumour area
6%
4%
2%
0%
n.s
C
DIFFERENTIATION
Ras^{V12}; scrib IR>
cherry IR
dorsal IR-1
GFP Elav
Differentiation ratio
Elav area in tumour / tumour area
60%
40%
20%
0%
***
D
SURVIVAL
Ras^{V12}; scrib IR>
cherry IR
dorsal IR-1
GFP cDcp1
Apoptosis ratio
cDcp1area in tumour / tumour area
3%
2%
1%
0%
***

Figure